Nd_2Fe_14B permanent magnets substituted with non-critical light rare earth elements (Ce, La): A review

Gérard Delette

$Nd_2Fe_{14}B$ permanent magnets substituted with non-critical light rare earth elements (Ce, La): A review

G. Delette

Univ. Grenoble Alpes, CEA, LITEN, DTNM, 38000 Grenoble, France

https://doi.org/10.1016/j.jmmm.2023.170768

Abstract

The growing demand in high performance Nd-Fe-B permanent magnets, driven by emerging key technologies, notably vehicles electrification and wind turbines, raises the question of the availability of critical raw materials, namely the Light Rare Earth Elements (LREEs) Nd and Pr. Co-extracted with these LREEs, Ce and La represent about 70 % of the total amount of rare earths in minerals and, for this reason, could constitute a cost-effective diversification in the raw materials sourcing for magnets. Largely unused and stored, these non-critical elements are progressively incorporated in the permanent magnet industry as a substitution of Nd and Pr, allowing a more balanced utilization of the resources. The restoration of high magnetic performances, after the substitution of Nd by Ce, constitutes, however, a considerable challenge that requires to re-design some steps of the conventional routes for producing dense anisotropic magnets. This objective has motivated a wide range of research activities during the last decade from which different approaches are now emerging: the Hot-Deformation technique followed by an infiltration of eutectic alloys, on the one hand, and, on the other hand, the powder pressing and sintering possibly completed with the Grain Boundary Restructuring or with the Grain Boundary Diffusion Process. The performances of Ce based magnets improved by these routes are analyzed for a wide range of substitution rates and compositions. The strategies specifically deployed in the powder metallurgy route for enhancing the coercivity and the remanence, based

on grain boundary engineering, additives alloying and on dual-powder sintering, are discussed in details.

Keywords: Permanent magnets, Nd-Fe-B, critical materials, substitution, Cerium

1. Introduction

Since their discovery in 1983, neodymium iron boron magnets with a hard magnetic phase made of the $Nd_2Fe_{14}B$ structure have become the most performant magnets produced at the industrial scale [1]. Besides major applications in automation, appliances, robotics, medical and industrial equipment, hard drive disks, Nd-Fe-B magnets tend to be widely used in electrical machines such as traction motors of electrical cars as well as generators for offshore wind turbines [2]. The commercial grades of magnets are classified by designers according to two relevant figures of merit, the energy product, or BH_{max}, and the coercivity, or H_{cJ}. The first quantity, expressed in kJ/m^3 or in MGOe, reflects the magnet strength, i.e., the magneto-static energy that can be provided in a magnetic circuit by a unit volume of a magnet. The second one reveals the resistance toward demagnetization, i.e., the maximal opposite field, expressed in kA/m or in kOe, that the sample can sustain before the cancellation of its polarization. Combined together by the simple addition of their values in CGS units, these physical quantities give rise to the so-called magic number (NM) that is useful to compare different processes. Current commercial Nd-Fe-B magnets can be supplied with BH_{max} values up to 56 MGOe (440 kJ/m^3) and coercive fields exceeding 1500 kA/m (19 kOe). A main concern regarding these high performance magnets is the utilization of critical elements, namely Nd, Pr and heavy rare earths such as Dy and Tb, that constitute about 30 % of the magnet weight. Considering the rapid growth expected within the decade of the magnet demand in order to comply with the transport electrification and the wind energy deployment [3], the replacement of Nd-Fe-B magnets with rare earth free [4], or with critical-rare-earth free compounds [5], [6] has become a great challenge. The investigation for the substitution of Nd in the $Nd_2Fe_{14}B$ structure with more abundant and less critical elements such as Ce, La and Y has intensified dramatically in the ten last year.

This review aims at compiling and analyzing the data collected from publications regarding different types of Ce-substituted magnets, including magnets manufactured at the industrial scale by the powder metallurgy route and by hot-deformation. Compared to the latest review [7], the survey covers recent results obtained on sintered magnets manufactured by dual-powder methods, Grain Boundary Restructuring and Grain Boundary Diffusion Process. The co-substitution of Nd with Ce and Y or La, as well as the effect of some additives are also reviewed in order to supply a large overview of the potential of such resource efficient magnets.

2. Cerium in rare earth permanent magnets

2.1 Rare earth sourcing

Rare Earth Elements (REEs) are co-extracted from natural deposits under the form of mineral species, mainly bastnaesite and monazite, and then separated in order to feed the demand of the current applications. Lanthanum and Cerium represent about 70 % of the weight of REEs present in the minerals but less than 10 % of the economic value of the whole REEs extracted [8]. Actually, Ce and La are devoted to industrial uses with low added values. For the mining sector, La and Ce are considered as by products with low economic value compared to the REEs used for permanent magnets (Nd, Pr, Sm, Dy) which constitute about 25 % of the REE content of the extracted minerals. The unbalance between the minerals composition and the market value is seen as a burden in the REE mining activity and several initiatives are considered for the valorization of Ce [8].

Cerium constitutes about 50 % of the REE content of minerals extracted from the site of Bayan Obo [9]. After separation, large amounts of unused Ce are currently stored which explains the lower price of Ce (5 $/Kg) compared to Nd (56 $/Kg in 2015). Magnet industry in China is following a policy toward a more balanced use of REEs involving research activities that aim to substitute Nd in Nd-Fe-B permanent magnets by the more abundant and cheaper La, Ce and

Y elements [9]. The large majority of the articles referenced in the Scopus database dealing with this topic have been published after 2012 (92 %), the share involving Chinese research groups represent 88 % of the total number of publications accepted in scientific journals over the same period. The progress obtained by Chinese groups have been presented in previous reviews [7], [10], [11] notably the concept of dual-powder sintering, called Multi Main Phase (MMP). This approach consists in mixing powders having different contents in Ce, one with high Ce content (Ce-Rich) and the second with low Ce substitution (Nd-Rich). After sintering, the microstructure exhibits interesting heterogeneities (concentration gradients) leading to higher performances compared to the single alloy approach implemented with the same average composition. Since 2015, Ce content magnets are commercially available with, for instance, the performance of N28 grades (H_{cJ} = 10.7 kOe) achieved for a substitution rate (Ce/RE) of 50 % and those of N38H (H_{cJ} = 16.2 kOe) grades fulfilled with Ce/RE = 20 % [7].

2.2 Atomic structure of Ce containing alloys

The crystalline structure $R_2Fe_{14}B$ (R = Y, Ce, La, Nd, Pr, Gd, Dy, Tb) is tetragonal and belongs to the spatial group $P4_2/mnm$. Each cell contains 68 atoms (4 formula) exhibiting 6 different sites for iron, two for the R element (R4f and R4g) and only one for the boron atom. For the compounds $(Nd_{1-x}RE_x)_2Fe_{14}B$, rare earth (RE) elements with an atomic radius smaller than the one of Nd preferentially occupy the RE4f sites which have a lower volume than RE4g sites [12]. In the case of $(Nd_{1-x}Ce_x)_2Fe_{14}B$, Colin et al. [13] experimentally observed that Ce atoms slightly tend to be located on R4f positions, which was consistent with recent ab initio calculations [14]. The smaller site R4f also favors the valence state Ce^{4+} which, due to the lack of electrons on the 4f layer, is a nonmagnetic form of Ce [15]. In the compound $Ce_2Fe_{14}B$, two valence states Ce^{3+}/Ce^{4+}coexist [7] and the averaged valence of Ce atoms is 3.44 [16]. Colin et al. [13] found that this value evolves slightly within the whole range of substitution in $(Nd_{1-}$

$_xCe_x)_2Fe_{14}B$, and, conversely to Alam et al. [17] who expected the occurrence of a phase separation from their ab initio calculations, they also observed the formation of the solid solution for all substitution rate values ($0 < x < 1$). These findings explain the so called dilution effect of Ce leading to a gradual reduction in the saturation magnetization M_s as the Ce content rises [18], [19] due to the very low magnetic moment carried by this element [20].

The trivalent nature of Ce, beneficial for the magnetization saturation, increases with the size of the host site [16], which, in turn, can be modified with some additive elements. Combined with Ce, Lanthanum contributes to rise the size of R sites, switching the valence state toward the Ce^{3+} form [15], [21], [22]. Consistently, Li et al. experimentally evidenced the raise in M_s with the La content in $[Ce_{1-x}La_x]_2Fe_{14}B$ alloys [7]. However, high content of La reduces the structural stability and the phase decomposition is observed for $x > 0.5$ [23].

3 Studies on rapid solidified alloys

The R-Fe-B alloys reviewed in this section have been obtained by the melt spinning process that is categorized as a rapid solidification technique. The starting ingots are firstly produced by arc melting with the desired composition. The ingots are then fused and rapidly solidified on the surface of a rotating wheel where they undergo a quenching with cooling rates up to $10^4 – 10^6$ $K.s^{-1}$ [24]. In the case of (Nd,Pr)-Fe-B alloys, the ejected ribbons feature a homogeneous nanostructure that can be partially crystallized by thermal treatments providing hard magnetic properties suitable for the production of permanent magnets. In their pioneering work, Croat et al. [25] noticed that the $Ce_{13.5}Fe_{81}B_{5.5}$ (at. %) melt spun alloys exhibited poor hard magnetic properties with coercive field close to 3 kOe. This performance was five times lower than the value of the $Nd_{13.5}Fe_{81}B_{5.5}$ counterpart (H_{cJ} ~ 15 kOe) [25] and reveals to be insufficient for most of permanent magnet applications. However, the analysis of ternary compounds Ce-Fe-B emphasized the effect of Ce on intrinsic and extrinsic properties of alloys.

3.1 Ce-Fe-B alloys

For the fully Ce substituting alloys, Herbst et al. [26] showed that the optimal magnetic properties are achieved for non-stoichiometric compositions, i.e. with an excess content of Ce. The optimal compositions belongs to the inner part of a triangular sector of the ternary diagram for which the 3 vertices correspond to the phases $CeFe_2$, $Ce_2Fe_{14}B$ and $Ce_{1.12}Fe_4B_4$ [27]. In that case, the rise is the Ce content favors the formation of the $CeFe_2$ phase at the expense of the boride Fe_3B which reduces severely the coercivity [28]. However, the amount of the hard magnetic T1 phase ($Ce_2Fe_{14}B$) is then reduced, down to 88% for instance in the $Ce_{17}Fe_{78}B_6$ (at. %) compound, i.e. to a level much lower than the one encountered in optimal Nd-Fe-B alloys (95 %). The paramagnetic $CeFe_2$ phase is detrimental for the remanence of ribbons but can be eliminated by thermal treatments [29], [30], [31], [24]. The infiltration of binary alloys NdCu and NdAg from the surface of the ribbons, performed by diffusion treatments, also improved the magnetic properties [32]. Applying these strategies, coercive fields of about 6 kOe and BH_{max} up to 8 MGOe have been reported on Ce-Fe-B melt spun ribbons (see **Table S1 in Supplementary Data**). It is worth noting that the higher coercive fields are achieved for Ce or (Ce+La+Y) contents of 17 at. % whereas, for the stoichiometric composition (RE = 12 at. %), the coercivity remains lower than 3 kOe (see **figure 1**).

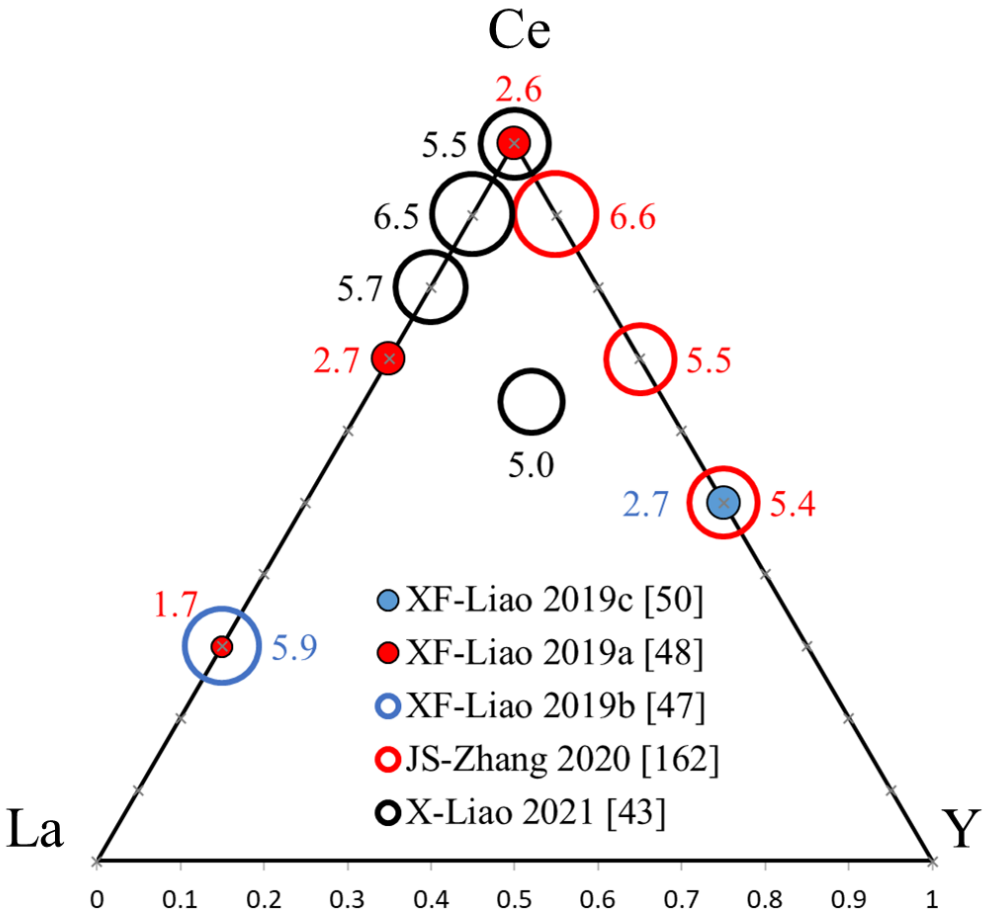

Figure 1: Coercive field H_{cJ} values reported in publications for melt-spun ribbons with the composition $(Ce_{1-y-z}La_yY_z)_{12+x}Fe_{72-x}B$ (x=0 solid circles, x=5 open circles). The sizes of the symbols correspond to the H_{cJ} value also indicated in kOe (data selected from Table S1 and Table S4)

3.2 (Nd,Ce)-Fe-B alloys

Early work of Croat at al. [25] showed that partially substituted melt spun ribbons with 20 % of Nd replaced by R = Ce or La in $(Nd_{0.8}R_{0.2})_{13.5}Fe_{81}B_{5.5}$ can exhibit interesting magnetic properties with H_{cJ} lying between 11 and 13 kOe. In such alloys, Ce as well as La atoms tend to be expelled from the T1 phase, resulting in a Nd content in this phase higher than the average value [33], [34]. Obviously, the Curie temperature decreases with the Ce content but with a rate found to be lower than the one expected from the mixture law. Ce atoms segregate at grains

boundaries and form the paramagnetic phase $CeFe_2$ that could promote grains exchange decoupling [35]. Hien et al. [36] measured an anisotropic field ($\mu_0 H_A$) value for the $(Nd_{0.8}R_{0.2})_{15}Fe_{77}B_8$ alloy of 4.2 T at room temperature and highlighted a strong decrease compared to the non-substituted $Nd_{15}Fe_{77}B_8$ alloy for which $\mu_0 H_A$= 8.2 T. The coercive field of $(Nd_{1-x}Ce_x)_2Fe_{14}B$ alloys depends on two antagonist effects: the dilution effect that reduces the anisotropic field of the T1 phase and the grain decoupling which prevents from a reversal propagation from grains to grains. The evolution of the magnetic properties with the substitution rate *x* is not monotonic: notably, BH_{max} and H_{cJ} are found to vary slowly within the range of $0.2 < x < 0.5$ [28], [37]. Other authors even observed an abnormal evolution of the coercivity which exhibits a peak for a *x* value that depends on the RE content [38], [39], [40], [34]. Those authors attributed this behavior to a separation of the main phase into Nd-Fe-B and Ce-Fe-B phases activated for a threshold in the Ce content. Yang et al. [40] noticed a variation of the lattice parameters in the main phase for $x = 0.2$ and ascribed this to a composition instability. The phase separation was also deduced by Zhou et al. [34] from their observation of a subdivision into cells of the main phase. However, those authors reported that the cells disappeared after an annealing treatment performed above 700°C. This temperature corresponds to the typical conditions required for the crystallization of ribbons [41]. Accordingly, Rong et al. [42] did not report an abnormal evolution of the magnetic properties with the Ce content in their annealed ribbons. The magnetic performances published on these alloys are collected in **Tables S2 and S3**. It is worth noting that coercive field values higher than 18 kOe have been achieved in the state of the art for a substitution rate of 20 %. These performances corresponds to a RE contents close to 31 % wt. This value of RE content reveals to be optimal within the whole range of the substitution rate (see **figure 2**).

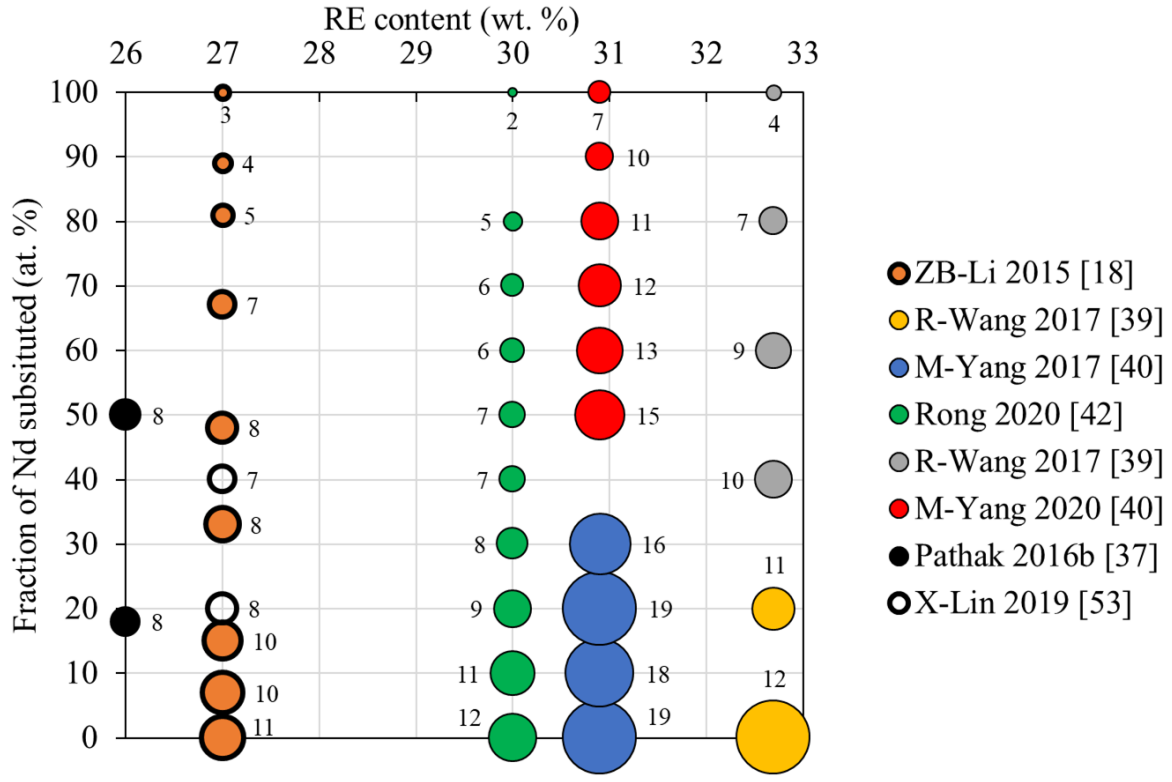

Figure 2: Coercive field H_{cJ} values reported in publications for melt-spun ribbons with the composition [Nd(Ce,La)]-Fe-B for various RE contents and substitution rates (solid circles: Ce substitution, open circles: Ce+La substitution). The sizes of the symbols correspond to the H_{cJ} value also indicated in kOe (data selected from Table S2, S3 and S6)

3.3 (Ce, La, Y, Gd)-Fe-B alloys

The crystallization of the $Ce_2Fe_{14}B$ structure reveals to be more difficult than $Nd_2Fe_{14}B$ and the alloy is prone to the formation of parasitic phases, such as $CeFe_2$, that affects the remanence. The poor stability of the magnetic properties with temperature, related to the low Curie point of the Ce alloy (T_c = 422 K), also constitutes the main drawback of $Ce_2Fe_{14}B$ compared to other $RE_2Fe_{14}B$ phases. The temperature stability of a magnet is quantified by two coefficients, namely $\alpha = \Delta B_r / B_r \Delta T$ and $\beta = \Delta H_{cJ} / H_{cJ} \Delta T$ that characterize the mean decrease in remanence B_r and coercivity H_{cJ}, within a given temperature amplitude, ΔT. For Ce-Fe-B melt spun

ribbons, the typical values of α lie between -0.6 and -0.4 %/K while β is comprised between -0.8 and -0.6 %/K (for ΔT = 400-300 K) [43].

For this reason, many published works aimed at partially replacing Ce by stabilizing elements, mainly Y, La and Gd. The magnetic performances of the melt-spun ribbons with different compositions of Ce, La, Y and Gd are listed in **Table S4**. Gadolinium addition contributes to a better crystallization of the T1 phase [44] and to a rise in the Curie temperature [45]. Lanthanum tends to destabilize the $CeFe_2$ phase with an actual benefit on the saturation magnetization [46] and energetic product [47], [48]. Conversely to La, Yttrium preferentially enters the T1 and raises the Curie point (T_c of $Y_2Fe_{14}B$ = 571 K). It also improves the remanence [49], owing to the stabilization of the amorphous phase during annealing, and also the coercive field stability with temperature [50]. Simultaneous replacement of a part of Ce by La and Y allows combining the beneficial effects of these two elements on the magnetic performances: a drastic reduction of the temperature coefficients have been found in [43] for $[(Ce_{0.7}La_{0.3})_{0.5}Y_{0.5}]_{17}Fe_{78}B_6$ (at. %) ribbons with α value attaining -0.17 %/K and β close to -0.08%/K within 300-400K.

3.4 (Nd,Ce,La)-Fe-B alloys

Liu et al. [51] showed that the co-substitution of Nd by Ce and La in melt-spun alloys limits the formation of $CeFe_2$, with a beneficial effect on the remanence. It also produces a finer microstructure in the ribbons after annealing. Lanthanum tends to segregate at grain boundaries [33], and when it replaces more than 30 % of Nd, the La used as a sole substitution element leads to the decomposition of the hard magnetic phase, conversely to the case where La is used with Ce [52]. Lin et al. reported that whatever the co-substitution rate of Nd with (Ce, La) in $[Nd_{1-x}(La_yCe_{1-y})_x]_2Fe_{14}B$ alloys, the magnetic performances are improved compared to the case with a single element substitution (Ce or La) [53]. For x = 0.2 and y = 0.4 they measured an energetic product of 15.1 MGOe on melt-spun ribbons whereas the value is reduced to 14.5

MGOe with $x = 0.2$ and $y = 0$. For higher substitution rates, the advantage of the co-substitution is more pronounced: a BH_{max} of 12.4 MGOe is obtained with $x = 0.5$ and $y = 0.4$ that compares favorably to the value of 8.2 MGOe obtained with $x = 0.5$ and $y = 0$ (see **Table S5**).

3.5 Hot deformed magnets

In the hot-deformation route, rapid quenched ribbons are crushed and processed into anisotropic dense magnets by a two-step technique involving a first hot pressing at 700°C followed by a second hot pressing allowing deformation perpendicular to the compaction direction (die-upsetting) [54]. This technique introduces a textured microstructure where the easy magnetization axes are preferentially oriented along the press direction. This so-called hot deformation process typically leads to energy product values larger than 40 MGOe for Nd-Fe-B alloys. Yoshida et al. [55] found that the Ce substitution in (Nd,Ce)-(Fe-Co)-B melt spun alloys improves the hot workability of the material. Using Misch-Metal based melt-spun ribbons, Ko et al. [56] achieved a coercive field value of 3.6 kOe and BH_{max} = 6.8 MGOe on die-upset samples , with a beneficial effect of Al and Co additions.

Pathak et al. [38] obtained a coercive field of 9.4 kOe on hot-deformed magnets with a substitution rate of 20 % of Nd by Ce. Poenaru et al. [57] observed similar performances and even noticed an improvement in coercivity for an higher substitution rate (30 %) attributed to the better workability of the alloy ascribed to the low melting temperature of the Ce-rich intergranular phase.

In order to improve the coercive field of hot deformed magnets, the infiltration of a liquid intermetallic phase (NdCu) was found to be remarkably efficient [58], [59], [60], [61]. The infiltration was performed around 700°C and aimed at creating a core shell structure in grains with a hard ferromagnetic shell enriched with Nd [58]. However, a detrimental soft ferromagnetic phase $(Nd,Ce)_6Fe_{13}Ga$ may form at grain boundaries upon NdCu infiltration with

a limitation of the gain in coercivity [59]. This secondary phase can however be suppressed by Co addition [60]. Eventually, by adjusting the RE content and the hot pressing temperature to avoid the formation of $CeFe_2$, Tang et al. [61] reported for Ce/RE = 20 % and after NdCu infiltration, a coercive field of 18.3 kOe for hot deformed anisotropic magnets (Br = 1.29 T, see **Table S6**).

4- Studies on sintered magnets

4.1 Conventional sintering process with (Nd,Ce)-Fe-B powders

The conventional powder metallurgy route for manufacturing high performance magnets relies on the alloy synthesis by Strip Casting (SC) followed by jet-milling in order to obtain fine monocrystalline powders prone to pressing and sintering [62]. The cooling rare during SC is suited to provide crystallized alloys without the formation of iron precipitates. The SC ribbons are mainly composed of well-defined T1 lamellas separated by a RE-rich phase [63]. A specific treatment under H_2, named Hydrogen Decrepitating (HD), is performed to transform this phase into brittle hydrides that subsequently improve the material pulverization.

Excepted the works of Yan et al. [64], [65] and Jin et al. [66] who studied respectively Strip Casting and Hydrogen Decrepitating performed on fully substituted alloys, the majority of publications deals with partially Ce substituted (Nd,Ce)-Fe-B sintered magnets. Actually, due to the low melting temperature of the $Ce_2Fe_{14}B$ phase (982 °C) compared to $Nd_2Fe_{14}B$ (1155°C), specific microstructures are formed in Ce-Fe-B ribbons by SC, quite differently from the well-defined lamellas of T1 phase found in Nd-Fe-B SC alloys. In Ce-Fe-B cast ribbons, core-shell microstructures are formed with a core made of $\alpha Fe/Fe_2B$ surrounded by a shell of T1 phase [65]. These structures coexist with the $CeFe_2$ phase. Addition of some RE, e.g. Ho, allows generating more conventional lamellas of the T1 phase in the solidified ribbons [64]. Yttrium also limits the αFe precipitation in such ribbons [67].

In (Ce,La)-Fe-B SC ribbons, $CeFe_2$ is limited but the oxidation of the RE-rich phase, exacerbated by La, hinders the subsequent reactivity with H_2 that would be suited for an efficient milling. Therefore, HD may require higher H_2 pressure to proceed such (Ce, La) based alloys compared to the Nd-Fe-B case [66].

For partially substituted alloys $(Nd_{1-x}\ Ce_x)$-Fe-B, Poenaru et al. [68] characterized the microstructure of strip-cast ribbons for $0 < x < 0.6$. They found that the $CeFe_2$ compound appears for $x = 0.3$ and is located between the T1 lamellas. This phase totally replaces the (Nd,Ce)-rich phase for $x = 0.6$ which would restrict the powder metallurgy route to lower Ce substitution rates.

Following the pioneering work of Sagawa et al. [69] on sintered Nd-Fe-B magnets, Okada et al. [70] published early studies on (Nd,Ce)-Fe-B magnets manufactured by the powder route and found that, owing to high RE contents (32.5 – 34.5 wt%), Ce favored the formation of a liquid phase, allowing the sintering temperature to be reduced under 1040°C. Tang et al. [71] showed that Al addition helps the formation of intergranular phases that also assist the sintering. In that case, the reduction of the sintering temperature favorably limits the grain growth, avoiding coercivity degradation that would occur in a large grained microstructure. The evolution of the magnetic performances of sintered $(Nd_{1-x},Ce_x)FeB$ magnets with the substitution rate (up of 56 %) has been firstly reported by Yan et al. [72]. For $x = 0.24$, they evidenced a continuous thin $CeFe_2$ phase (2-5 nm) located at grain boundaries that acts positively on grains decoupling and counterbalances the detrimental effect on coercivity due to the Ce dilution. In a later study, the same group reported that the decrease in H_{cJ} with the temperature is lower after Ce substitution: at 150°C and, for $x = 0.24$, the coercive field is equivalent to the value measured on magnets without Ce [73]. Jin et al. [74] established that the $CeFe_2$ phase forms during the sintering and thermal annealing steps, since the Laves phase is not observed on the strip-cast precursors for $x = 0.25$. The segregation of the $CeFe_2$ phase at

grain boundaries is accompanied by the formation of a core-shell structure into grains featuring a Nd-rich shell, also reported in the work of Chen et al. [75], and attributed to the expulsion of Ce atoms from the T1 grain phase. However, Enokido et al. [76] pointed out that the Ce-containing phases, liable to segregate at grain boundaries, may have a detrimental ferromagnetic character (inducing grain coupling), depending on the Ce content: $(Nd,Ce)Fe_2$ compound becomes actually paramagnetic for high Ce content whereas the $(Nd,Ce)_6Fe_{13}Ga$ follows the opposite trend. Consequently, the beneficial effect of Ga addition on coercivity is more pronounced for low Ce substitution rates. As for melt-spun alloys, some authors investigated the substitution of Nd with Y and La. Fan et al. [77] established that Y, conversely to Ce, tends to enter the T1 phase, reducing the intrinsic performances of the T1 phase $(Nd_{1-x},Y_x)_2Fe_{14}B$. However, in a later work, the same group noticed that Nd atoms, when replaced by Y in the grains, tend to form RE-rich (decoupling phases) at grain boundaries. For $x = 0.2$, they noticed an overall improvement of the coercive field [78]. The same group noticed, as for melt-spun alloys, that Y substitution improves the thermal stability of Ce substituted magnets [79]. When used as a single substituting element, La, like Ce, is expelled from the T1 phase but tends to concentrate at triple junctions without leading to a continuous decoupling phase distribution at grain boundaries [77]. Without heavy rare earth addition and for a moderate ratio Ce/RE= 20 %, the best performances reviewed in literature for sintered magnets lie between 10 and 12 kOe for H_{cJ} and between 36-41 MGOe for BH_{max}, disregarding the commercial grades (see **Table S7**). This corresponds to a Magic Number (MN) value of about 50-55. The **figure 3** allows an overview of magic numbers extracted from different sources as a function of the RE content and substitution rates. Commercial grades and hot-deformed magnets performances are also plotted for comparison.

4.2 Conventional sintering process with Misch-Metal powders

Misch-Metal (MM) can be directly produced from the extracted minerals with the following typical RE content: Ce (55%), La (25%), Nd (15%), Pr (5%). Utilization of MM alloys in magnets could be interesting since it would avoid the expensive RE separation required after mining [80]. According to references [81], [82] magnets with the composition MM33Fe66B (wt %) could cover a range of BH_{max} values between 10 and 20 MGOe. Niu et al. [82] stated that large amount of $CeFe_2$ phase forms and remains stable for the MM composition and, in practice, the BH_{max} is lower than 10 MGOe (**see Table S8**). Shang et al. [83] reported that the La is expelled to the grain boundaries where it tends to be oxidized. Compared to the content in the initial MM, the La deficit in the T1 phase inside the grains is about 7.5 %. Liu et al. [80] determined that the $CeFe_2$ content is 4.7 % in mass for MM33Fe66B sintered magnets. This phase tends to form large precipitates at Triple Junctions (TJs) which hinders the densification [82]. To overcome this effect, some authors suggested either to reduce the MM share by diluting MM-Fe-B powders with (Nd, Pr)-Fe-B powders, with ratios MM/TR < 50% [84] or to increase the La content to destabilize the $CeFe_2$ phase [82], [85]. For instance, with MM/RE = 30% and (Ce/RE = 17%, La/RE = 9%), Yu et al. [85] reported the following performances: BH_{max} of 37.8 MGOe and H_{cJ} = 7.6 kOe. Alternatively, Liu et al. [86] obtained with MM/RE = 100 % a BH_{max} value of 20.6 MGOe after a Grain Boundary Diffusion Process with TbH_x.

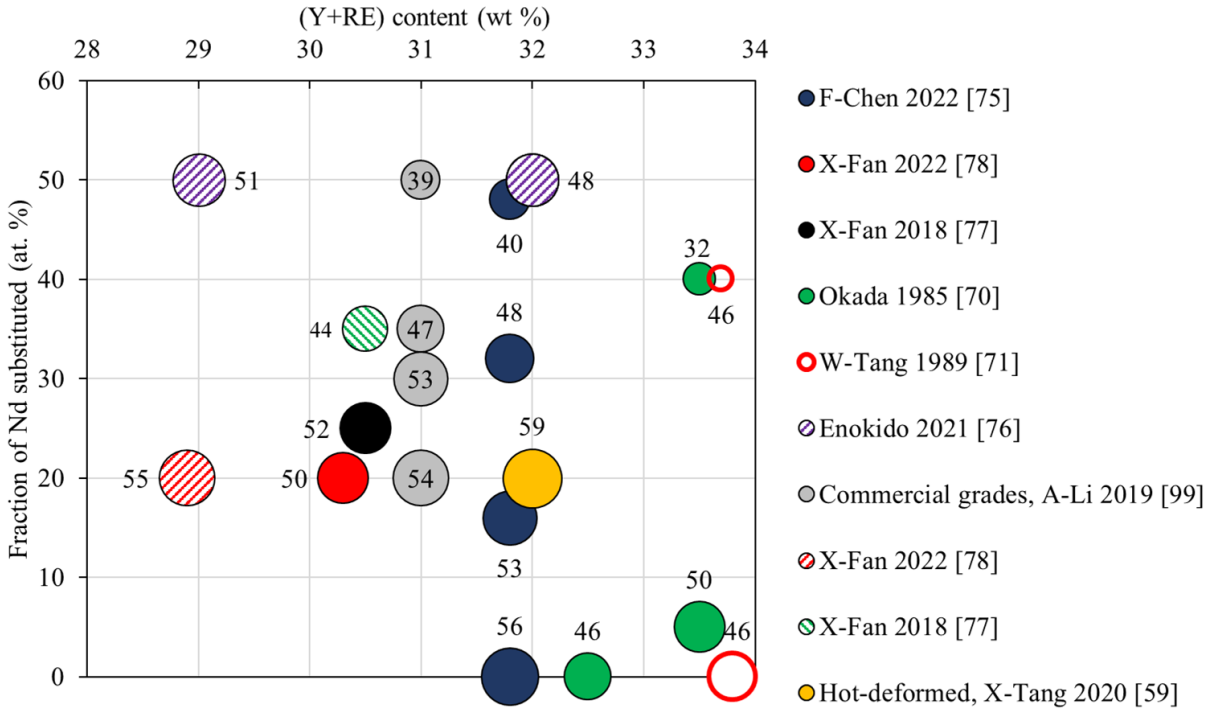

Figure 3: Magic Number MN values (BH_{max} [MGOe]+H_{cJ} [kOe]) of sintered magnets (SMP) extracted from publications for various RE contents and substitution rates (solid circles: Ce substitution, open circles: Ce+La substitution, dashed circles: Ce+Y substitution). The sizes of the symbols correspond to the MN value also indicated in dedicated unit (data selected from Table S8).

4.3 Multi Main Phase (MMP) process

In 2014, Zhu et al. [87] published early results based on the co-sintering of two powders, the one being Nd-Rich (without Ce substitution) and the second being Ce-Rich, introducing the MMP process. Their samples exhibited a moderate reduction in the coercive field due to the Ce content: for an average ratio Ce/TR of 20 %, the coercivity remained better than 12 kOe with BH_{max} = 45 MGOe. They concluded that the decrease in the performances with Ce substitution in MMP is less than the one previously measured by Zhou et al. [88] in Ce substituted magnets processed by the single powder approach (named Single Main Phase or SMP in the following). Zhu et al. [87] stated that, in the MMP process, fine grained microstructure can be more easily

obtained after sintering. Actually, larger amount of Ce is segregated at GBs in MMP which lowers the melting temperature of the RE rich phases. The sintering temperature can thus be reduced owing to the contribution of the liquid phase to the densification. Eventually, the grain growth, with a detrimental effect on the coercivity, can be avoided during sintering. In MMP magnets, copper addition is found to improve the GB wetting by the (Nd,Ce)-rich phase which contributes to develop the coercivity during thermal annealing [89]. However, especially in the MMP process, oxygen content should be carefully controlled due to the higher affinity of O_2 with Ce than with Nd [90]. Even for low oxygen contents, Huang et al. [89] noticed the formation of fcc phases $(Nd,Ce)O_x$ in which O atoms are in solid solution. In a subsequent work, Zhu et al. [91] compared the performances of magnets with Ce/RE = 20 % sintered by the MMP and SMP techniques. They reported a coercive field of 12.1 kOe for MMP, much higher than 7.7 kOe for the conventional approach and they correlated this result with a higher amount of intergranular phases with MMP. The published results regarding MMP magnets performances are listed in **Table S9**.

Numerous studies have been published in the recent years to explain the higher coercivity found in MMP sintered magnets. Fan et al. [92] provided more details of the intergranular microstructure with the evidence of an amorphous phase, 3 nm thick, around the grains in MMP, whereas this intergranular phase is not observed in the SMP case. This phase is expected to contribute to the grain decoupling in MMP. Moreover, Han et al. [93] reported that the structure of the phase at TJs belongs to the dhcp type in MMP magnets, with a lower iron content compared to the SMP counterpart where the TJ phase exhibits a fcc structure. They argued that the lattice parameter mismatch between TJ-dhcp-phase and T1 phase is lower than the one between TJ-fcc-phase and T1 which is beneficial for mitigating the nucleation of the demagnetization at the interface between T1 and TJ phases. Besides such differences noticed in the structure of intergranular phases, Fan et al. [92] inferred that a shielding effect from hard

grains could explain the better coercivity in MMP: the magnetization reversal in low coercive Ce-rich grains could be delayed owing to their magnetic coupling with higher coercive Nd-rich grains. This idea is also supported by the work of Zhang et al. [27] who observed core-shell structures in grains with a Nd enrichment in the shells of the Ce-rich grains. This group stated that such structures are generated by the interdiffusion of Ce and Nd atoms through the liquid RE-rich phase at GBs provided that the liquid phase forms a percolating network [94]. These authors estimated that the $CeFe_2$ introduced in the mixture by the Ce-Rich powder, with a melting point at 925°C, contributes more efficiently to the liquid sintering and to the wetting of grain boundaries than in the SMP case for which less $CeFe_2$ is available [27]. The effect on the coercive field, related to a better distribution of the Laves phase $Ce(Fe,Co)_2$ in MMP magnets, is confirmed by Chen et al. [95]. The gap in coercivity, 11.4 kOe (MMP) vs 10.4 (SMP), is however less pronounced in the work of Zhang et al. [27] than in the previous study of Zhu et al. [91]. In a very different approach for preparing MMP powders, based on high energy ball milling of RE oxides precursors followed by H_2 reduction, Zhu et al. [96] obtained, by mixing after reduction Nd-rich and Ce-rich powders, an higher coercive field (H_{cJ} = 4.5 kOe) compared to the case where the oxides precursors were mixed before milling (H_{cJ} = 1.7 kOe).

Further studies investigated the effect of thermal annealing performed on MMP sintered magnets. In the conventional sintering process, such thermal treatments aims at improving the distribution of intergranular phases around grains and at promoting the magnetic decoupling. Zhang et al. [97] showed that an high annealing temperature activates the RE atoms diffusion and tends to smoothen the concentration gradients left after the sintering between Ce-rich and Nd-rich grains. Above 580°C, the coercivity decreases and at 880°C, they found that Ce and Nd heterogeneities tend to disappear and the coercivity becomes close to the value measured in SMP magnets. Liu et al. [51] determined the composition of RE-rich phase at GBs after annealing and reported that the iron content raises, at the expense of RE, as the temperature

rises: at 410°C the iron content is 30% whereas it raises to 50% at 460°C. The reduction of the RE content is detrimental for the coercivity due to a poorer wettability and a more ferromagnetic character of the intergranular phase. Jin et al. [98] suggest skipping the post sintering thermal treatments for MMP magnets.

Micro-magnetic simulations of Li et al. [99] supports the beneficial effect on the coercivity of the heterogeneous microstructures encountered in MMP magnets, provided that the inter-diffusion of Nd and Ce atoms is non-symmetrical. Those authors assumed that Nd atoms enter more easily the T1 phase than Ce atoms, arguing that $Ce_2Fe_{14}B$ phase is less stable. This results in the formation of Nd-rich shells in Nd-Lean grains by a diffusion that is not balanced by an equivalent formation of Ce-rich shells. Considering that Nd shells harden the Ce-rich grains, their calculation supports the higher coercive field found in MMP compared to SMP (**figure 4**).

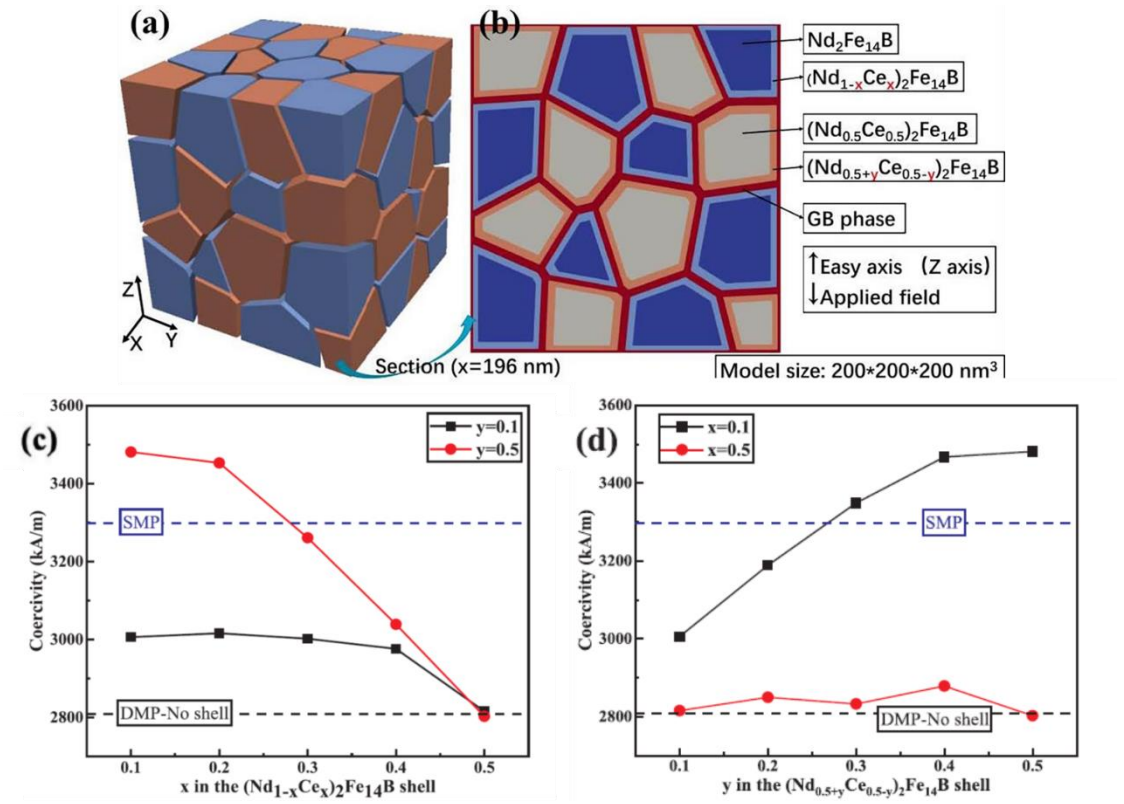

Figure 4: Micromagnetic simulation of the demagnetization curve of MMP (DMP) and SMP sintered magnets, MMP is made by a mixture of 50% of grains with the initial composition $(Nd_{0.5}Ce_{0.5})_2Fe_{14}B$ *and 50 % of grains with the initial composition* $Nd_2Fe_{14}B$*, SMP is made of identical grains with the average composition, after sintering, interdiffusion of Ce and Nd is assumed to have generated shells with various composition in MMP grains (a) The 3D simulation model consists of 64 irregular grains separated by GB phase. The* $Nd_2Fe_{14}B$ *grains are blue and* $(Nd_{0.5}Ce_{0.5})_2Fe_{14}B$ *grains are yellow. The volume fraction of* $(Nd_{0.5}Ce_{0.5})_2Fe_{14}B$ *shown in this figure is 50%. (b) The section (x = 196 nm) in the simulation model. Shells with varied RE ratios form at the surface of the grains. The red region is grain boundaries. The deep yellow region and light blue region is the shells. (c) the dependence of the coercivity on y in the* $(Nd_{0.5+y}\ Ce_{0.5-y}\ )_2Fe_{14}B$ *shell for x=0.1, 0.5. (d) the dependence of the coercivity on x in the* $(Nd_{1-x}Ce_x)_2Fe_{14}B$ *shell for y=0.1, 0.5. MMP exhibits higher coercivity than SMP counterpart for strong dissymmetrical diffusion, i.e; for high y values and low x values (from Li et al.* [99]*).*

4.4 Multi Main Phase (MMP) process with multiple substitutions

As for the conventional process (SMP), multiple substitutions with Ce, La and Y have been investigated for the MMP process. Co-substitution with Ce and La elements are often considered with a ratio Ce/La = 65/35 that corresponds to the minerals natural content. The authors expected a gain on the thermal stability owing to the higher Curie temperature of $La_2Fe_{14}B$ (T_c = 530 K). Combined with the MMP process, the La/Ce co-substitution has also been found to improve the mechanical properties of magnets [15], due to the better ductility of the $REFe_2$ phase, as well as the corrosion behavior [100], owing to the role of $REFe_2$ precipitates that limit the penetration of electrolyte along GBs. As mentioned before, the co-substitution (Ce,La) allows tailoring the amount of $REFe_2$ phase which could be excessive when Ce-rich alloys are used in MMP [101], [98], [102], [103]. Wei et al. compared MMP magnets made with Ce (Ce/RE = 25%) and with Ce/La ([Ce,La]/RE = 25%) and showed that the La limits the $REFe_2$ amount, meaning more T1 phase and better remanence (BH_{max} = 39.5 MGOe vs 37.8 MGOe). The La expelled at GBs also improves the wettability of the intergranular phase with a gain in coercivity (H_{cJ} = 8.8 kOe vs 6.9 kOe). Increasing the amount of the total RE content of MMP magnets ([Ce,La]/RE = 40%) by adding a third powder (Nd-rich) has also been found to improve the coercivity [104].

Chen at al. [105] investigated MMP magnets for which the (Ce,La)-rich powder was made with a mixture of Misch-Metall-based powder (50%) and Nd-Fe-B powder (50%) leading to the average ratio: MM/RE = 35% (Ce/RE = 19%, La/RE = 10 %). The results (BH_{max} = 38.2 MGOe, H_{cJ} = 11 kOe) are similar to the performances reported by Jin et al. [98] for MMP magnets for which the (Ce,La)-rich powder was homogeneous. As for a single Ce substitution in MMP, for which the annealing tends to homogenize the microstructure, the co-substituted (Ce,La) MMP magnets are also prone to a decrease in their coercivity upon annealing [105].

The co-substitution with Ce and Y in MMP magnets has been analyzed by Peng et al. [106] who reported that, conversely to La, Y actually enters the T1 leading to an increase in T_c. Li et al. [67] extended the substitution to the group R' = Ce, La, Y and Gd. They noted with the MMP approach that Nd and Y are localized at the grains periphery and they obtained interesting performances H_{cJ} = 5.57 kOe and BH_{max} = 20.17 MGOe for a substitution rate of R'/(R'+Nd) = 75%.

Liu et al. [107] performed micro-magnetic simulations to explain the role of magnetic coupling between grains by the intergranular phase in MMP magnets. They considered in their model two grain populations: Nd-rich grains with high coercivity and (Ce,La) grains with low coercivity. The two populations are mixed in different ratios to achieve two cases (low and high Ce/La average contents). In the low (Ce,La) content magnet (9%), the grains can be considered to be magnetically coupled due to the low amount of RE-rich intragranular phase. The coercivity is then found to be tailored by the lowest switching field value, i.e. by the softer (Ce,La)-rich grains. For the high (Ce,La) content case (36%), despite the dilution effect, the grains are better decoupled since the amount of RE-rich phase is larger and the coercivity is found to depend on the harder phase. The combination of all these effects accounts the slight difference of the coercivity experimentally measured between the two samples despite the large gap in the (La,Ce) content. Interestingly, for a given substitution rate (La,Ce)/Nd = 40% in the MMP magnets, Chen et al. [104] showed that the increase in the total RE content (La,Ce,Nd), from 30.8 to 33.8 wt. %, led to a rise in the coercivity (H_{cJ} shifted from 7.27 to 11.1 kOe). In their RE-rich magnets, the thicker Nd enriched shells encountered in grains combined with Nd-rich phases at GBs explain the better performances.

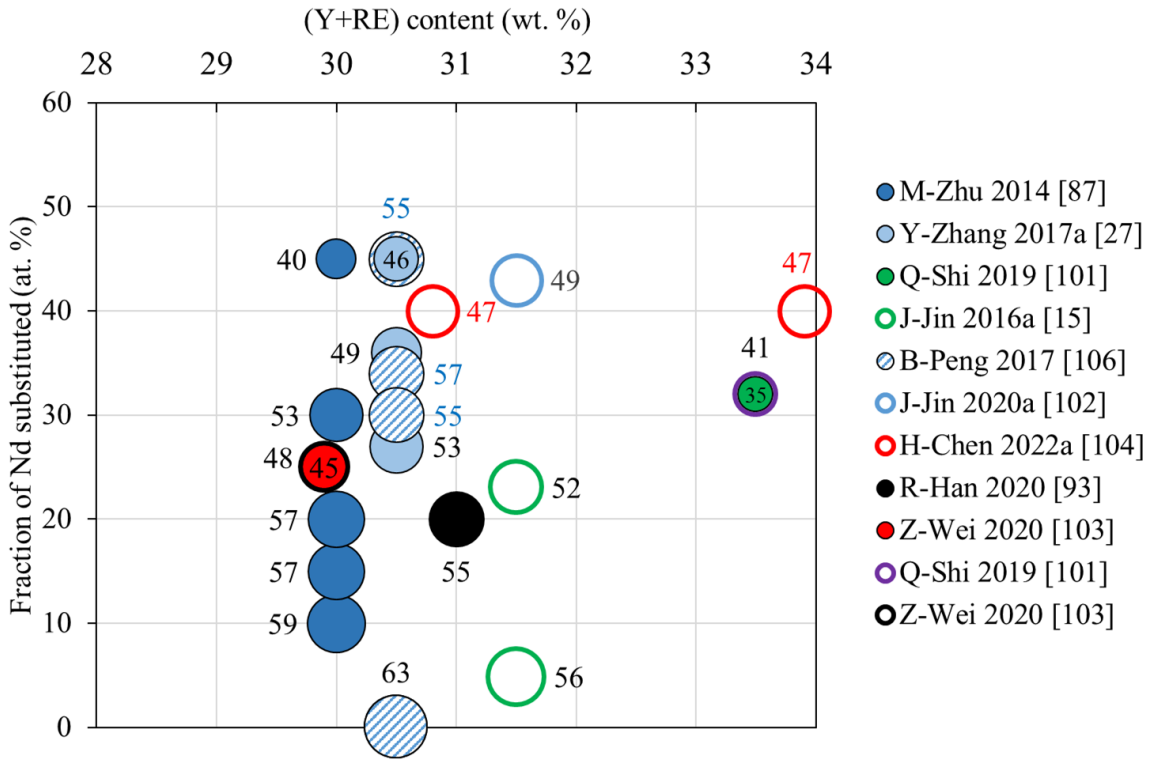

Figure 5: Magic Number MN values (BH_{max} [MGOe] + H_{cJ} [kOe]) of sintered magnets (MMP) extracted from publications for various RE contents and substitution rates (solid circles: Ce substitution, open circles: Ce+La substitution, dashed circles: Ce+Y substitution). The sizes of the symbols correspond to the MN value also indicated in dedicated unit (data selected from Table S9).

4.5 Grain Boundary Restructuring (GBR)

Grain Boundary Restructuring approach has been studied both for SMP and MMP process and the corresponding data are compiled in **Table 1** and **Table 2,** respectively. GBR consists in the modification of the structural and/or chemical features of the intergranular phases [108]. These phases result from the RE excess introduced in the RE-Fe-B alloys and evolve during sintering and annealing in combination with some elements (Cu, Co, Al, Ga,…). With GBR, an additional powder with high RE content and/or low melting temperature is mixed with the RE-Fe-B powder before sintering. This powder could be made of intermetallic alloys such as NdFe

[109], (Nd,Pr)Al [110], CeAl [111], PrFeAlGa [112], RE hydrides (Nd,Pr)H_x [113], [114], [115], [116], [117], [118], [119], or Nd-rich Nd-Fe-B alloy [104]. Associated with the MMP process, the interaction of the additional powder with the majority phases is driven by the heterogeneous microstructure of these magnets. Actually, the Nd atoms, introduced for instance by a diluted NdH_x powder, tends to diffuse preferentially into the Ce-rich grains, increasing the dissymmetric diffusion of Ce and Nd already noticed in MMP. As reported below, once replaced by Nd, Ce tends to segregate at GBs forming the $REFe_2$ phase [118] and could also induce a better resistance toward corrosion by limiting the access of the electrolyte to the GBs [119]. With the Nd addition by GBR, the RE-rich phase contents more Nd and less Fe improving the magnetic decoupling [116], [117]. For the special case of PrFeAlGe powder addition, the non-magnetic compounds RE_6Fe_{13}(Al,Ga) forms at GBs allowing the La atoms, that would otherwise be oxidized, to be consumed [112].

The works of Ma et al. [114], [116] give a comparison of the performances obtained with the NdH_x-GBR approach carried out with SMP and MMP magnets for Ce/RE = 27%. With an addition of 2 % of NdH_x powder, the magic number (BH_{max} [MGOe] + HcJ [kOe]) has been found to rise by 0.6 for SMP magnets [114] and 2.7 for MMP magnets [116]. The higher remanence found with MMP is attributed to the preferential replacement of Ce by Nd in Ce-rich grains (see **figure 6).**

The gain in performances with the GBR method is generally lower that the one provided by the Grain Boundary Diffusion Process (GBDP) [118], [120]. Liu at al. [118] showed that, in their experiment, the GBDP gives larger improvement in terms of coercivity (H_{cJ} = 14.2 kOe vs 10.2 kOe for GBR) and energy product (BH_{max} = 38.5 MGOe vs 33.9 MGOe for GBR). Actually, the $CeFe_2$ phase that develops with GBR reduces the remanence due to the iron consumption whereas this phase is not observed in case of GBDP. Moreover, Nd-rich shells in Ce grains,

resulting from Nd diffusion, are thicker after GBDP near the magnet surface which provides a shielding effect to the magnet.

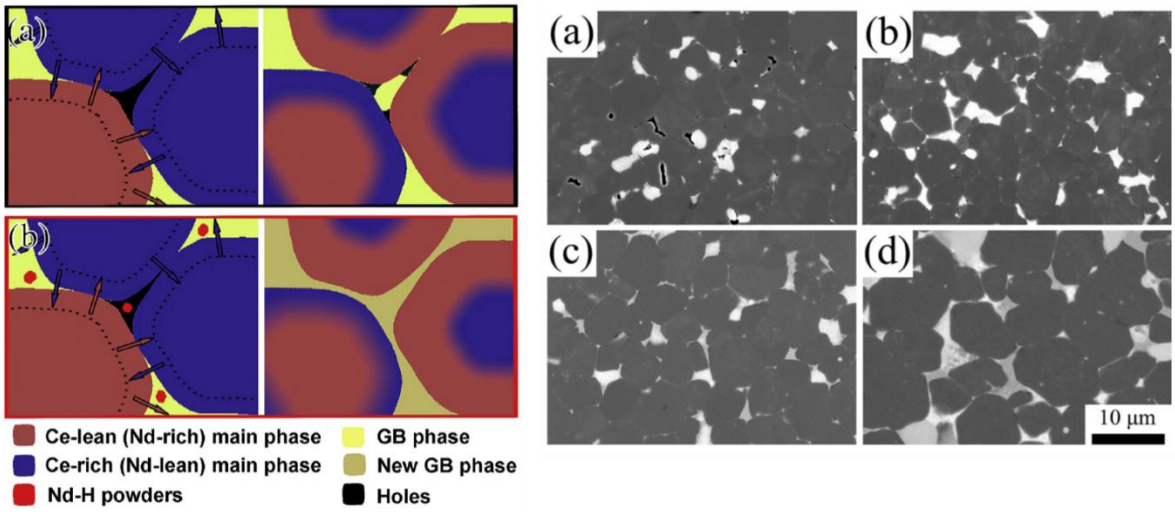

Figure 6: Schematic illustrations for the evolution of microstructure and elemental interdiffusion for the MMP starting magnet. (a) and the magnet added with NdHx (b), based on elemental distribution mapping revealing larger enrichment of Nd in Ce-rich grains compared to the Ce-enrichment in Nd-rich grains with an amplification of the effect after NdH_x addition at GBs (left). Low magnification back-scattered SEM images for the starting magnet (a), the magnets added with 2 wt.% (b), 3 wt.% (c) and 4 wt.% (d) NdHx (right, from T-Ma et al. 2018 [116])

4.6 Grain Boundary Diffusion Process (GBDP)

Since the early work of Park et al. [121], the Grain Boundary Diffusion Process has been widely implemented for improving the coercivity of Nd-Fe-B magnets with a rationale use of Heavy Rare Earth (HRE: Dy, Tb). The process consists in coating the surface of the sintered magnets with HRE compounds and performing a thermal treatment allowing the HRE element to penetrate into the magnet, preferentially along the GBs [122]. The temperature is adjusted around 900°C to form a liquid phase at GBs but also to limit the diffusion of the HRE into the grains. This results in a core-shell structure at the grain scale featuring a hard magnetic shell

owing to the partial substitution of Nd by HRE in this area. In the case of Ce substituted magnets, published works depict mostly the implementation of intermetallic alloys and hydrides (TbH_x in [123]) as diffusing species (see **Table 3** for GBDP with SMP magnets and **Table 4** for MMP magnets). The intermetallic phase contain generally one or two RE elements amongst (Nd, Pr, Dy, Tb) combined with one or several elements belonging to the group (Al, Cu, Fe, Ga). These last elements are selected for improving the GB wettability, e.g. Al [124], [34], for enhancing the corrosion resistance, e.g. Cu [125] and for forming nonmagnetic $RE_6Fe_{13}Ga$ phases at GBs [125], [126], [127]. The addition of light rare earth elements (Nd, Pr) aims at rising the RE content in the intergranular phase, improving the decoupling and, in turn, enhancing the coercivity without using HRE [128], [129], [120], [125], [126]. Chen et al. [128] compared the performances obtained with NdCu and DyCu alloys on SMP magnets and stated that HRE based alloy did not provide a better coercivity after GBDP. The same trend was shown by Jin et al. [129] who tested PrAl and PrDyAl alloys on SMP magnets. In the second case, they concluded that the Dy segregated at the magnet surface and is therefore inefficiently employed. GBDP performed on waste Ce-substituted magnets for restoring the performance was conducted with a PrTbCu ternary alloy [130]. The authors reported that the Tb is consumed by the T1 phase and penetrates only over 300 µm whereas Pr enters the intergranular RE-rich phase and diffuses deeply in the magnet. Upon GBDP, the distribution of $CeFe_2$ precipitates formed in high Ce content magnets may act unfavorably, since this phase tends to absorb the HRE elements and limits its penetration [131], [132]. This deleterious effect can be reduced if the diffusion treatment is performed above 925°C, i.e. when the elimination of the $CeFe_2$ occurs via the reaction $Ce_2Fe_{14}B + CeFe_2 \rightarrow L + Ce_2Fe_{17}$. This condition also promotes the penetration of HRE through the liquid phase at GBs [123]. However, as previously mentioned, the elevation of the temperature should be avoided for MMP magnets because the (Nd, Ce) interdiffusion may induce an homogenization of the microstructure [125]. Zhang et al. [133] obtained the best

results on MMP magnets (Ce/RE = 20 %) ever published after a diffusion treatment performed at 900°C/10h with Tb: the coercivity raised from 12.48 kOe to 20.08 kOe whereas BH_{max} was maintained at 38.5 MGOe (see **Table 4**).

4.7 Spark Plasma Sintering (SPS)

Conversely to conventional sintering, Spark Plasma Sintering permits the densification of RE-Fe-B powders at lower temperatures, around 700-800°C, compared to the standard conditions (1000-1060°C). This technique keeps the monocrystalline and coercive structure of powders produced after the milling of melt-spun ribbons [134]. Several authors studied the mixture of two nanocrystalline powders (Ce-rich and Nd-rich from Magnequench) densified by SPS and reported, as for the MMP process, a beneficial effect on the performances resulting from the heterogeneous microstructure [135], [136], [137] (see **Table S10**). Grain Boundary Restructuring also reveals to be efficient for developing core-shell structures during SPS consolidation, either with NdCu [138], PrCu [135] or DyF_3/Cu addition [137]. Cui et al. obtained with this approach coercive field values up to 15 kOe with high a substitution rate Ce/TR of 40 % [135].

5 Role of additive elements

The role of additives elements in R-Fe-B alloys has been intensively investigated in order to improve both the intrinsic properties (coercive field and Curie temperature), via the element substitution in the T1 phase, and the extrinsic properties (remanence, coercivity) owing to the formation of secondary phases [139]. The following reviewed data are more specifically related to the intrinsic properties adjustments reported for Ce substituted alloys.

5.1 Co addition

Co improves the Curie temperature of Ce substituted magnets with, for instance, a gain of 90°C for the composition $Ce_3Fe_{14-z}Co_xB$ between $z = 0$ and $z = 2$. The solubility of Co into the $Ce_2Fe_{14}B$ phase is limited and higher Co contents ($z > 2$) may forms parasitic secondary phases [140]. According to Pathak et al. [37], in the partially substituted alloys $(Nd_{1-x}Ce_x)_{2+y}Fe_{14-z}Co_zB$, Co atoms preferentially occupy the Fe4c site and shift the valence of Ce from (4+) to (3+). Therefore, they found that Co addition also improved the energy product of melt-spun ribbons from 10.6 to 16 MGOe with $z = 2$.

5.2 Zr and Hf addition

For Jurczyk et al., Zr [141] and Hf [142] atoms can replace RE atoms in the T1 structure and enhance the magneto-crystalline anisotropy at the expense of the Curie temperature. In the case of $Ce_{17}Fe_{78-x}Zr_xB_6$ (at%) melt-spun alloys, a rise in coercivity is reported for $x = 0.5$ [143] as well as in the case of $Ce_{17}Fe_{78-x}Hf_xB_6$ (at%) for $x = 1$ [144]. Excessive addition of Zr should be avoided since it tends to form ZrB_2 borides and subsequently the parasitic Ce_2Fe_{17} phase due to the boron consumption [145], [146]. However, such borides, under the form of nanoprecipitates, are liable to limit the grain growth during sintering. This pinning effect allows the sintering temperature to be adjusted in order to obtain full densification and better magnetic properties [147], [148]. Ta, Nb and Mo are also mentioned to help the microstructure refinement in (Ce,Nd)-Fe-B alloys [149], [150].

5.3 Si and Al addition

Silicon partially substitutes iron in $Ce_2(Fe_{14-x}Si_x)B$ alloys with a lattice parameter reduction. With 0.6 at % Si, the Curie temperature rises by 30°C [151]. Li et al [152] found in their early work that addition of 1 at% Si in (NdCe)(FeSi)B alloys improves the coercivity. This effect

was attributed to an increase in the magneto-crystalline anisotropy for Ce substituted magnets [88], [153]. Addition of Al (and Mo) has also been found to improve the magneto-crystalline anisotropy of alloys made with Misch-Metall with on optimum for x = 0.05 for the composition $MM_2Fe_{14-x}Al_xCo_2B$ [154].

Zhang et al. [153] studied the compositions $Ce_{17}Fe_{78-x}Si_xB_6$ and stated that Si could also destabilize the $CeFe_2$ phase for $x > 1.5$ with a benefit in terms of remanence. Si could thus be combined with La for this purpose [155]. The same effect has been reported with Ti [156] and Ge additions [157].

5.4 Ga and Cu addition

Beside the formation of the $RE_6Fe_{13}Ga$ phase at GBs, Ga partially substitutes iron in $Ce_{17}Fe_{78-x}B_6Ga_x$ alloys and shifts the Ce valence toward the magnetic form Ce^{3+} [158]. The substitution also improves the Curie temperature. Conversely to Ga, copper is slightly soluble in the T1 phase and segregates at GBs where it lowers the melting temperature of secondary phases. Without Cu addition, Xi et al. reported that the $REFe_2$ phase is more concentrated at TJs [159] rather than being efficiently distributed along GBs. However, an excessive Cu addition could increase the Nd content of the $REFe_2$ phase that exhibits ferromagnetic characteristics, at the expense of the coercivity. In the $(Nd_{0.5}Ce_{0.5})_{30.5}Fe_{68.5-x}Cu_xB$ (at. %) alloys, the optimum coercivity is achieved for $x = 0.2$ [160].

6 Summary

The substitution of Nd by non-critical rare earth elements (Ce, La) inevitably reduces the performances of the Nd-Fe-B hard magnetic compound mainly due to the lower intrinsic properties of the T1 phases made of Ce and La. Some strategies have been proposed to mitigate the deleterious effect of the substitution. Regarding the alloys composition, it has been

demonstrated that an excess in rare earth content and the Co addition limit the formation of some detrimental secondary phases at the expense of $REFe_2$ that distributes at grain boundaries. This compound consumes iron atoms and induces a penalty on the remanence, but, owing to its low melting point, $REFe_2$ assists the sintering and favors the grain decoupling due to the its paramagnetic nature. Lanthanum destabilizes the Laves phase $REFe_2$ and is efficient to tailor the amount of $CeFe_2$ phase for high substitution rates.

Ce atoms substitutes Nd in the $RE_2Fe_{14}B$ structure with two possible valence states $Ce^{3+/}Ce^{4+}$, but the small volume of the substitution sites in the lattice favors the Ce^{4+} form. This structural evolution accounts for the dilution effect of the magnetic properties directly related to the non-magnetic moment carried by the Ce^{4+} form. Co-substitution with La, Y or Gd partially restores the properties of the hard magnetic phase. However, the coercivity of (Ce, La) substituted magnets has been more efficiently enhanced by the grain boundary engineering techniques. These approaches mainly consists in developing intergranular secondary phases, with a non-ferromagnetic nature, spread around the hard phase to promote the magnetic exchange-decoupling between adjacent grains. Infiltration, Grain Boundary Restructuring and Grain Boundary Diffusion Process are designed for that purpose with significant results. It is worth noting that these techniques could also magnetically harden the grains owing to the insertion of (Nd, Dy, Tb) that improve the anisotropic field into thin shells.

Regarding more specifically the powder metallurgy route, the dual powder sintering approach, also named Multi Main Phase (MMP), reveals to be attractive. The heterogeneous microstructures provided by MMP have been found to be more coercive than the homogeneous counterpart obtained with single powder sintering. This technique exploits the difference in structural stability of the Ce and Nd T1 phases characterized by a trend for the Ce to be expulsed to the grain boundary whereas Nd atoms prefer enter the T1 phase. Two favorable effects on

the coercive field are derived: the enrichment of Nd in Ce-lean grains and a higher amount of paramagnetic $REFe_2$ at GBs.

Increasing above 40 % the substitution rate of Nd with (Ce, La) in magnets, while maintaining sufficient performances, will be challenging in the next years. This may involve to better predict and to screen the magnetic properties of a wide range of [(R-R'),Nd]-Fe-M-B structures (R =Ce, La, Gd, Y) including various alloying elements (R' in RE sites or M in Fe sites) to optimize the intrinsic properties, notably the anisotropic field.

Acknowledgments

Part of this work has been performed in the frame of the European Project LowREEMotors funded by EIT Raw Materials.

Figure captions

Figure 1: Coercive field H_{cJ} values reported in publications for melt-spun ribbons with the composition $(Ce_{1-y-z}La_yY_z)_{12+x}Fe_{72-x}B$ (x=0 solid circles, x=5 open circles). The sizes of the symbols correspond to the H_{cJ} value also indicated in kOe (data selected from Table S1 and S4).

Figure 2: Coercive field H_{cJ} values reported in publications for melt-spun ribbons with the composition [Nd(Ce,La)]-Fe-B for various RE contents and substitution rates (solid circles: Ce substitution, open circles: Ce+La substitution). The sizes of the symbols correspond to the H_{cJ} value also indicated in kOe (data selected from Table S2, S3 and S6).

Figure 3: Magic Number MN values (BH_{max} [MGOe].+ H_{cJ} [kOe]) of sintered magnets (SMP) extracted from publications for various RE contents and substitution rates (solid circles: Ce substitution, open circles: Ce+La substitution, dashed circles: Ce+Y substitution). The sizes of the symbols correspond to the MN value also indicated in dedicated unit (data selected from Table S8).

Figure 4: Micromagnetic simulation of the demagnetization curve of MMP (DMP) and SMP sintered magnets, MMP is made by a mixture of 50% of grains with the initial composition $(Nd_{0.5}Ce_{0.5})_2Fe_{14}B$ and 50 % of grains with the initial composition $Nd_2Fe_{14}B$, SMP is made of identical grains with the average composition, after sintering, interdiffusion of Ce and Nd is assumed to have generated shells with various composition in MMP grains (a) The 3D simulation model consists of 64 irregular grains separated by GB phase. The $Nd_2Fe_{14}B$ grains are blue and $(Nd_{0.5}Ce_{0.5})_2Fe_{14}B$ grains are yellow. The volume fraction of $(Nd_{0.5}Ce_{0.5})_2Fe_{14}B$ shown in this figure is 50%. (b) The section (x = 196 nm) in the simulation model. Shells with

varied RE ratios form at the surface of the grains. The red region is grain boundaries. The deep yellow region and light blue region is the shells. (c) the dependence of the coercivity on y in the $(Nd_{0.5+y}\ Ce_{0.5-y})_2Fe_{14}B$ *shell for x=0.1, 0.5. (d) the dependence of the coercivity on x in the* $(Nd_{1-x}Ce_x)_2Fe_{14}B$ *shell for y=0.1, 0.5. MMP exhibits higher coercivity than SMP counterpart for strong dissymmetrical diffusion, i.e; for high y values and low x values (from Li et al.* [99]*).*

Figure 5: Magic Number MN values (BHmax [MGOe].+ HcJ [kOe]) of sintered magnets (MMP) extracted from publications for various RE contents and substitution rates (solid circles: Ce substitution, open circles: Ce+La substitution, dashed circles: Ce+Y substitution). The sizes of the symbols correspond to the MN value also indicated in dedicated unit (data selected from Table S9).

Figure 6: Schematic illustrations for the evolution of microstructure and elemental interdiffusions for the MMP starting magnet. (a) and the magnet added with NdHx (b), based on elemental distribution mapping revealing larger enrichment of Nd in Ce-rich grains compared to the Ce-enrichment in Nd-rich grains with an amplification of the effect after NdH_x *addition at GBs (left). Low magnification back-scattered SEM images for the starting magnet (a), the magnets added with 2 wt.% (b), 3 wt.% (c) and 4 wt.% (d) NdHx (right, from T-Ma et al. 2018* [116]*).*

Table captions

Table 1: Magnetic properties of sintered magnets SMP after GBR

Table 2: Magnetic properties of sintered magnets MMP after GBR

Table 3: Magnetic properties of sintered magnets SMP after GBDP

Table 4: Magnetic properties of sintered magnets MMP after GBDP

Table 1: Magnetic properties of sintered magnets SMP after GBR

Composition (wt %)	Additive elts in alloy M (w%) / Compound used in GBR (wt%)	Σ TR wt%	Σ TR at%	at. Ce /TR	at. (Nd+Pr) /TR	Br (T)	[BH]max [MGOe]	Hc (kOe)	Δ NM (*)	Δ Hc (kOe)	Reference
Nd19.1Ce10.9Fe67.5M1.5B	M : Al, Cu, Nb, Co	30	13.6	0.37	0.63	1.25	35.5	10.56			K-Chen 2017a [109]
	Nd90Fe10 (1%)	30.6	14	0.36	0.64	1.26	35.8	11.30	1.04	0.74	
	Nd90Fe10 (2%)	31.2	14.3	0.35	0.65	1.24	34.2	12.00	0.14	1.44	
	Nd90Fe10 (3%)	31.8	14.7	0.34	0.66	1.22	33.4	12.10	-0.56	1.54	
Nd10.1Ce19.6Fe69.3B1.1	M : any	29.7	13.5	0.67	0.33	1.1	11	1.90			L-Zhang 2017 [113]
	NdHx(4%)	32.52	15.1	0.58	0.42	1.03	20	5.10	12.20	3.20	
	NdHx(15%)	40.25	19.9	0.42	0.58	0.9	16.7	8.20	12.00	6.30	
Nd17.8Pr4.5Ce8.24Fe67.2M1.3B	M : Cu, Al, Ga, Zr	30.5	14	0.27	0.73	1.28	39.3	10.60			T-Ma 2017 [114]
	NdPrHx(1%)	31.2	14.3	0.27	0.73	1.27		12.00			
	NdPrHx(2%)	31.9	14.7	0.26	0.74	1.24	37.8	12.70	0.60	2.10	
	NdPrHx(3%)	32.6	15.2	0.25	0.75	1.2		12.90			
Nd18.3Pr4.57Ce7.63Fe67.5M1B	M : Al, Ga, Zr	30.5	14	0.26	0.74	1.28	39.3	10.60			J-Jin 2021 [115]
	NdPrHx(2%)	31.89	14.7	0.24	0.76	1.27		12.00			
	NdPrHx(1.8%) - Cu(0.2%)	31.69	14.7	0.24	0.76	1.24	37.8	12.70	0.60	2.10	
Nd18.2Pr6.06Ce8.2Fe65.13M1.6B	M : Al (1.2) – Cu (0.2) – Zr (0.2)	32.30	14.8	0.26	0.74						F-Xia 2022 [110]
	Nd60Pr20Al20(3%)	33.73	15.5	0.24	0.76	1.2	37.3	14.93			
NdFeB commercial grade (N52M)	M : not given					1.44	51.4	14.90			YJ-Wong 2022 [111]
	GBDP Tb70Cu30					1.41	49.8	22.70	6.20	7.80	
	Ce85Al15(2%)					1.37	46.9	16.30	-3.10	1.40	
	Ce85Al15(2%) + GBDP Tb70Cu30					*1.24*	*44.9*	*25.10*	*3.70*	*10.20*	
	Ce85Al15(4%)					1.29	41.5	17.10	-7.70	2.20	
	Ce85Al15(4%) + GBDP Tb70Cu30					*1.28*	*40.6*	*22.90*	*-2.80*	*8.00*	
	Ce85Al15(6%)					1.22	37.3	18.20	-10.80	3.30	
	Ce85Al15(6%) + GBDP Tb70Cu30					*1.19*	*35.7*	*24.40*	*-6.20*	*9.50*	

Table 2: Magnetic properties of sintered magnets MMP after GBR

Composition (wt %)	Additive elts in alloy M (w%) Compound used in GBR (wt%)	Σ TR wt%	Σ TR at%	at. Ce /TR	at. La /TR	at. (Nd+Pr) /TR	Br (T)	[BH]max [MGOe]	Hc (kOe)	Δ NM (*)	Δ Hc (kOe)	Reference
(NdPr)22.3Ce8.24Fe67.5M1B	M : Al, Cu, Ga, Zr	30.5	13.9	0.27	0	0.73	1.29	40	8.20			T-Ma 2018
	NdHx (1%)	31.2	14.3	0.27	0	0.73	1.28	39	10.10	0.90	1.90	[116]
	NdHx (2%)	31.9	14.7	0.26	0	0.74	1.28	39.7	11.20	2.70	3.00	
	NdHx (3%)	32.6	15.1	0.25	0	0.75	1.21	35.1	12.40	-0.70	4.20	
	NdHx (4%)	33.3	15.6	0.24	0	0.76	1.19	33.9	13.10	-1.20	4.90	
(NdPr)18.3Ce12.2Fe67.5M1B	M : Al, Cu, Ga, Zr	30.5	14	0.37	0	0.63	1.25	36.5	8.30			T-Ma 2018
	NdHx (3%)	32.6	15.2	0.41	0	0.59	1.22		12.20		3.90	[116]
Nd14.4Pr3.66La4.27Ce7.93Fe67.2M1.3B	M : Al, Cu, Co, Ga, Zr	30.5	14.00	0.26	0.14	0.59	1.29	34.9	5.07			Y-Liu 2021
	NdPrHx (1%)	31.2	14.50	0.26	0.14	0.61	1.27		8.93		3.86	[118]
	NdPrHx (2%)	31.9	14.90	0.25	0.13	0.62	1.23		9.58		4.51	
	NdPrHx (3%)	32.6	15.20	0.24	0.13	0.63	1.21	33.9	10.16	4.09	5.09	
	NdPrHx (4%)	33.3	15.60	0.23	0.13	0.64	1.20		10.79		5.72	
Nd14.64Pr3.66Ce12.2Fe67.1M1.4B	M : Al, Cu, Ga, Zr	30.5	14	0.41	0	0.59	1.27	37.9	8.70			J-Jin 2022
	NdPrHx (1%)	31.20	14.5	0.39	0	0.61	1.26	37.4	10.70	1.50	2.00	[119]
	NdPrHx (2%)	31.89	14.8	0.38	0	0.62	1.25	36.5	11.80	0.20	1.10	
	NdPrHx (3%)	32.59	15.2	0.37	0	0.63	1.24	35.9	12.50	0.30	1.80	
Nd21.3La3.2Ce5.95Fe67.13Cu1.44B0.93	M : Al, Cu, Co, Zr	30.50	14.00	0.20	0.11	0.69	1.27	38.48	12.30			S-Fan 2022a
	Pr82.2Fe6.1Ga9.53Al2.21 (2%)	31.53	14.70	0.19	0.10	0.71	1.26	38.05	13.90	1.17	1.60	[112]
	Pr82.2Fe6.1Ga9.53Al2.21 (4%)	32.57	15.30	0.18	0.10	0.73	1.22	34.91	17.20	1.33	4.90	
	Pr82.2Fe6.1Ga9.53Al2.21 (6%)	33.60	16.00	0.17	0.09	0.74	1.2	34.13	18.10	1.45	5.80	
	Pr82.2Fe6.1Ga9.53Al2.21 (8%)	34.64	16.40	0.16	0.09	0.76	1.17	32.8	19.90	1.92	7.60	

Table 3: Magnetic properties of sintered magnets SMP after GBDP

Composition (wt %)	Additive elts in alloy M (w%) / Compound used in GBDP (wt%)	R' wt%	R' at%	at. Ce /R'	at. La /R'	at. Y /R'	at Gd /R'	at. (Nd+Pr) /R'	Br (T)	[BH]max [MGOe]	Hc (kOe)	Δ NM (*)	Δ Hc (kOe)	Reference
Nd24.1Ce7.4Fe67.5B1.0	M : any	31.5	14.5	0.24	0	0	0	0.76	1.03		8.6			Q-Zhou 2018
	GBDP Nd80Al10Cu10								1.02		12.7		4.1	[34]
(NdPr)9.5Ce14.5Gd7.3Fe66.3M1.4B	M : Al (1.1) - Co (0.2) - Cu (0.1)	31.3	14	0.48	0	0	0.21	0.51	0.95		2.51			F-Chen 2020a
	GBDP Nd70Cu30								0.944		9.55		7.04	[128]
	GBDP Dy70Cu30								0.927		9.79		7.28	
Nd22.1Ce9.5Fe65.5M2.02B0.96	M : Al, Cu, Ga, Zr	31.5	14.6	0.31	0	0	0	0.69	1.16	32.2	7.4			Z-Li 2020a
	GBDP TbHx								1.15	34.3	9.5	4.2	2.1	[131]
Nd22.1Ce5.7La3.8Fe65.5M2.02B0.96	Al, Cu, Ga, Zr	31.5	14.6	0.18	0.12	0	0	0.7	1.15	31.4	14.6			
	GBDP TbHx								1.19	33.9	18.3	6.2	3.7	
Nd6.3Ce21.7Gd4.1Fe64.5M2.14B1.3	M : Co,Al,Cu,Zr,Nb	32.1	14.7	0.69	0	0	0.12	0.19		12.5	2.37			HB-Feng 2021
	GBDP TbHx									19.5	6.53	11.2	4.16	[123]
commercial magnets														
(Pr, Nd)25.77Ce5.88Fe66.55B0.95M0.85 N45	M : Cu, Ga	31.65	14.5	0.18	0	0	0	0.82	1.339	45	12.71			R-Du 2022
	GBDP TbFe								1.301		22.17		9.46	[127]
	GBDP Tb								1.272		22.09		9.38	
Ce14.5(Nd,Pr)9.5Gd7.3Fe66.5M1.4B	M : Al (1.1) - Cu (0.1) - Co (0.2)	31.2	14	0.47	0	0	0.3	0.23	0.95		7.3			F-Chen 2020a
	GBDP NdCu								0.944		9.55		2.25	[128]
	GBDP DyCu								0.927		9.79		2.49	
N28	M : not given			0.55				0.45		28	9			Q-Zhu 2020
	GBDP Tb										11		2	[132]
N33	M : not given			0.45				0.55		33	10.6			Q-Zhu 2020
	GBDP Tb										13		2.4	
N35	M : not given			0.3				0.7		35	10.9			Q-Zhu 2020
	GBDP Tb										15		4.1	[132]
Ce20	M : not given			0.2				0.8	1.2		10.1			M-Tang 2017
	GBDP Nd80Al20								1.2		12.5		2.4	[124]
	GBDP Nd60Dy20Al20								1.2		17.2		7.1	
	GBDP Nd40Dy40Al20								1.2		14.9		4.8	
	GBDP Nd20Dy60Al20								1.2		15.2		5.1	
	GBDP Dy80Al20								1.2		14.3		4.2	
Waste (Nd,Ce,Gd)FeB magnets (N30)	not given								1.08	25.4	9.59			Y-Liu 2020b
	GBDP Pr40Tb30Cu30								1.1	27.76	16.17	8.9	6.58	[130]

Table 4: Magnetic properties of sintered magnets MMP after GBDP

Composition (wt %)	Additive elts in alloy M (w%) Compound used in GBDP (wt%)	Σ TR wt%	Σ TR at%	at. Ce /TR	at. La /TR	at. Dy /TR	at. (Nd+Pr) /TR	Br (T)	[BH]max [MGOe]	Hc (kOe)	Δ NM (*)	Δ Hc (kOe)	Reference
Nd25.28Ce6.32Fe66.33M1.1B0.97	Cu, Al, Co, Nb, Ga	31.6	14.6	0.21	0	0	0.79	1.318	41.08	12.16			L-Zhang-2019
	GBDP Dy							1.314	40.83	16.96	4.6	4.8	[133]
Nd25.28Ce6.32Fe66.33M1.1B0.97	Cu, Al, Co, Nb, Ga	31.6	14.6	0.21	0	0	0.79	1.308	40.88	12.48	0.1	0.32	
	GBDP Tb							1.295	40.63	17.67	5.1	5.51	
Nd25.28Ce6.32Fe66.33M1.1B0.97	Cu, Al, Co, Nb, Ga	31.6	14.6	0.21	0	0	0.79	1.309	40.58	12.29	-0.4	0.13	
	GBDP TbF3							1.307	40.59	15.24	2.6	3.08	
Nd18.3Ce7.93La4.27M1B1	Cu, Ga, Zr	30.5	14	0.26	0.14	0	0.6	1.266		5			J-Jin 2020
	GBDP Pr80Al20							1.26		14.8		9.8	[129]
	GBDP Pr40Dy40Al20							1.216		15		10	
Nd14.6Pr3.7Ce7.9La4.3Fe67.5M1B	Al, Cu, Ga, Zr	30.5	14	0.26	0.14	0	0.6	1.29	34.9	5.2			Yo-Liu 2020
	GBDP (PrNd)Hx							1.29	38.5	14.2	12.6	9	[120]
	GBR (NdPr)Hx (3%)							1.21	33.9	10.2	4.0	5	
Nd14.6Pr3.7Ce7.9La4.3Fe67.2M1.3B	Co, Al, Cu, Zr, Ga	30.5	14	0.26	0.14	0	0.6	1.29	34.9	5.2			M-Yan 2022
	GBDP Pr80Ga20							1.31	41.4	16.1	17.4	10.9	[126]
Commercial magnets													
Nd17.11Pr3.34Ce7.39Dy0.26Fe69.3M1.6B	M : Co (0.41) – Nb (0.28) – Mn (0.12) – Al (0.42) – Si (0.13) – Cu (0.17) – Ti (0,04) – Zr (0.02)	28.1	12.6	0.27	0	0.01	0.72	1.23		11.66			J-Wang 2020 [125]
	GBDP Pr90Ga10							1.23		13.01		1.35	
	GBDP Pr90Ga7.5Cu2.5							1.23		14.82		3.16	

Supplementary data – Tables caption

Table S1: Magnetic properties of Ce-Fe-B melt spun ribbons

Table S2: Magnetic properties of (Nd,Ce)-Fe-B melt spun ribbons (Ce/RE < 40 %)

Table S3: Magnetic properties of (Nd,Ce)-Fe-B melt spun ribbons (Ce/RE > 40 %)

Table S4: Magnetic properties of (Ce, La, Y, Gd)-Fe-B melt spun ribbons

Table S5: magnetic properties of (Nd, Ce, La)-Fe-B melt spun ribbons (from [53])

Table S6: magnetic properties of (Nd, Ce)-Fe-B hot-deformed magnets

Table S7: Magnetic properties of sintered magnets SMP

Table S8: Magnetic properties of sintered magnets SMP with MM

Table S9: Magnetic properties of sintered magnets with MMP

Table S10: Magnetic properties of sintered magnets by SPS

Table S1: Magnetic properties of Ce-Fe-B melt spun ribbons

Composition wt %	Ce wt. %	Ce at. %	Br (T)	[BH]max [MGOe]	HcJ [kOe]	Reference
Ce35Fe64B	35	17	0.49	4.1	6.2	Herbst 2012 [26]
Ce30Fe68B	30	14	0.53	4.6	5.4	Herbst 2012 [26]
Ce27Fe72B	27	12	0.45	1.5	1.6	Herbst 2012 [26]
Ce28Fe71B	28	13	0.48	2.5	3.1	Herbst 2012 [26]
Ce23Fe76B	23	10	0.87	2.45	2.88	Grigorias 2017 [29]
Ce27Fe72B	27	12	0.82	5.71	3.96	Grigorias 2017 [29]
Ce31Fe69B	31	14	0.77	8.21	6.08	Grigorias 2017 [29]
Ce34Fe65B	34	16	0.66	6.33	6.21	Grigorias 2017 [29]
Ce35Fe64B	35	17	0.69	8.6	6.2	QY-Zhou 2015 [30]
Ce26Fe71B	26	12		7.31	4.43	Z-Li 2016 [28]
Ce32Fe67B	32	15		5.7	6.54	Z-Li 2016 [28]
Ce34Fe65B	34	16	0.47	4.14	4.61	LZ-Zhao 2017 [31]
Ce33Fe66B	33	16	0.49	4.77	6.17	X-Tan 2017 [24]
Ce27Fe72B	27	12	0.57	2.9	2.8	ZY-Zhang 2017 [161]
Ce27Fe72B	27	12		5.57	3.15	ZB-Li 2015 [18]
Ce30Fe69B	30	14	0.4	3.36	2.28	Rong 2020 [42]
Ce28Fe71B	28	13		7.31	4.43	Z-Li 2016 [28]
Ce32Fe67B	32	15		5.7	6.54	Z-Li 2016 [28]
Ce27Fe72B	27	12	0.57	3.6	2.6	XF-Liao 2019a [47]
Ce33Fe66B	33	15	0.54	2.7	3.66	R-Wang 2017 [39]
Ce31Fe68B	31	14	0.44		5.5	M-Yang 2017 [40]

Table S2: Magnetic properties of (Nd,Ce)-Fe-B melt spun ribbons (Ce/RE < 40 %)

Composition (wt %)	RE wt %	RE at%	Ce/ RE	Br T	[BH]max MGOe	HcJ kOe	Reference
Nd27Fe72B	27	12	0		21.06	10.94	ZB-Li 2015 [18]
(Nd0.93Ce0.07)27Fe72B	27	12	0.07		18.1	10.4	ZB-Li 2015 [18]
(Nd0.85Ce0.15)27Fe72B	27	12	0.15		17.33	9.61	ZB-Li 2015 [18]
(Nd0.67Ce0.33)27Fe72B	27	12	0.33		16.06	8.44	ZB-Li 2015 [18]
Nd33Fe66B	32.7	15	0	0.81	16.56	12.1	R-Wang 2017 [39]
(Nd0.8Ce0.2)33Fe66B	32.7	15	0.2	0.76	13.48	10.8	R-Wang 2017 [39]
Nd31Fe68B	30.9	14	0	0.84		19	M-Yang 2017 [40]
(Nd0.9Ce0.1)31Fe68B	30.9	14	0.1	0.75		17.5	M-Yang 2017 [40]
(Nd0.8Ce0.2)31Fe68B	30.9	14	0.2	0.7		19	M-Yang 2017 [40]
(Nd0.7Ce0.3)31Fe68B	30.9	14	0.3	0.65		15.5	M-Yang 2017 [40]
Nd30Fe69B	30	14	0	0.8	24.92	12.3	Rong 2020 [42]
(Nd0.9Ce0.1)30Fe69B	30	14	0.1	0.75	21.12	11.23	Rong 2020 [42]
(Nd0.8Ce0.2)30Fe69B	30	14	0.2	0.71	13.54	9.41	Rong 2020 [42]
(Nd0.7Ce0.3)30Fe69B	30	14	0.3	0.67	11.94	8.23	Rong 2020 [42]
(Nd0.8Ce0.2)30Fe59Co10B	30	14	0.2		12.6	17.7	Pathak 2015 [38]
(Nd0.82Ce0.18)26Fe62Co11B	26	11	0.18		16	7.7	Pathak 2016b [37]
(Nd0.8Ce0.2)27Fe72B	27	12	0.2	0.86	14.5	8	X-Lin 2019 [53]
(Nd0.7Ce0.3)27Fe72B	27	12	0.3	0.85	12.6	7.6	X-Lin 2019 [53]

Table S3: Magnetic properties of (Nd,Ce)-Fe-B melt spun ribbons (Ce/RE > 40 %)

Composition (wt %)	RE wt %	RE at%	Ce/ RE	Br T	[BH]max MGOe	HcJ kOe	Reference
(Nd0.6Ce0.4)33Fe66B	32.7	15	0.4	0.69	13.65	9.56	R-Wang 2017 [39]
(Nd0.4Ce0.6)33Fe66B	32.7	15	0.6	0.72	9	9.1	R-Wang 2017 [39]
(Nd0.2Ce0.8)33Fe66B	32.7	15	0.8	0.66	6.4	6.9	R-Wang 2017 [39]
Ce33Fe66B	32.7	15	1	0.54	2.7	3.66	R-Wang 2017 [39]
(Nd0.6Ce0.4)31Fe68B	30.9	14	0.4	0.62		15	M-Yang 2020 [40]
(Nd0.5Ce0.5)31Fe68B	30.9	14	0.5	0.6		13	M-Yang 2020 [40]
(Nd0.4Ce0.6)31Fe68B	30.9	14	0.6	0.55		12	M-Yang 2020 [40]
(Nd0.3Ce0.7)31Fe68B	30.9	14	0.7	0.54		11	M-Yang 2020 [40]
(Nd0.2Ce0.8)31Fe68B	30.9	14	0.8	0.52		9.5	M-Yang 2020 [40]
(Nd0.1Ce0.9)31Fe68B	30.9	14	0.9	0.49		7	M-Yang 2020 [40]
Ce31Fe68B	30.9	14	1	0.44		5.5	M-Yang 2020 [40]
(Nd0.6Ce0.4)30Fe69B	30	14	0.4	0.64	9.9	7.48	Rong 2020 [42]
(Nd0.5Ce0.5)30Fe69B	30	14	0.5	0.59	7.78	6.61	Rong 2020 [42]
(Nd0.4Ce0.6)30Fe69B	30	14	0.6	0.57	6.51	6.04	Rong 2020 [42]
(Nd0.3Ce0.7)30Fe69B	30	14	0.7	0.54	5.67	5.52	Rong 2020 [42]
(Nd0.2Ce0.8)30Fe69B	30	14	0.8	0.5	4.97	4.68	Rong 2020 [42]
Ce30Fe69B	30	14	1	0.4	3.36	2.28	Rong 2020 [42]
(Nd0.6Ce0.4)27Fe72B	27	12	0.4	0.86	13.5	6.8	X-Lin 2019 [53]
(Nd0.52Ce0.48)27Fe72B	27	12	0.48		14.39	7.68	ZB-Li 2015 [18]
(Nd0.33Ce0.67)27Fe72B	27	12	0.67		12.17	6.84	ZB-Li 2015 [18]
(Nd0.19Ce0.81)27Fe72B	27	12	0.81		10.86	5.18	ZB-Li 2015 [18]
(Nd0.11Ce0.89)27Fe72B	27	12	0.89		8.08	4.05	ZB-Li 2015 [18]
Ce27Fe72B	27	12	1		5.57	3.15	ZB-Li 2015 [18]
(Nd0.5Ce0.5)26Fe67Co5B	26	12	0.5		14.6	8	Pathak 2016b [18]
(Nd0.41Ce0.59)27Fe73B	27	12	0.59	0.95	17.84	10.6	M-Zhang 2018 [41]

Table S4: Magnetic properties of (Ce, La, Y, Gd)-Fe-B melt spun ribbons

Composition (wt %)	Ce+R' wt%	Ce+R' at%	at. Ce/ (Ce+R')	at. La /(Ce+R')	at. Y /(Ce+R')	at. Gd /(Ce+R')	Br T	[BH]max MGOe	Hc kOe	Reference
Ce28Fe71B	28	13	1	0	0	0		7.31	4.43	Z-Li 2017 [44]
Ce26Gd2Fe70B	28	13	0.93	0	0	0.07		6.75	5.88	Z-Li 2017 [44]
Ce27Fe72B	27	12	1	0	0	0	0.57	3.6	2.6	XF-Liao 2019a [48]
Ce8La197Fe72B	27	13	0.7	0.3	0	0	0.69	6.2	2.73	XF-Liao 2019a [48]
Ce8La197Fe72B	27	13	0.3	0.7	0	0	0.58	2.6	1.72	XF-Liao 2019a [48]
Ce22La9Fe68B	31	14	0.3	0.7	0	0	0.5	6.3	4.33	XF-Liao 2019b [47]
Ce24.5La10.5Fe64B	35	16	0.3	0.7	0	0	0.4	4.7	5.89	XF-Liao 2019b [47]
Ce27Fe72B	27	12	1	0	0	0	0.88	6.8	1.86	XF-Liao 2019c [50]
Ce14Y9Fe77B	23	12	0.5	0	0.5	0	0.75	6.2	2.66	XF-Liao 2019c [50]
Ce19Y12Fe67SiB	31	17	0.5	0	0.5	0		7.1	5.43	JS-Zhang 2020 [162]
Ce26Y7Fe65SiB	33	17	0.7	0	0.3	0		4.5	5.52	JS-Zhang 2020 [162]
Ce32Y2Fe63SiB	34	16	0.9	0	0.1	0		3.9	6.63	JS-Zhang 2020 [162]
Ce35Fe64B	35	17	1	0	0	0		4.32	5.5	X-Liao 2021 [43]
Ce32La3Fe64B	35	17	0.9	0.1	0	0		4.3	6.53	X-Liao 2021 [43]
Ce28La7Fe64B	35	17	0.8	0.2	0	0		5.44	5.69	X-Liao 2021 [43]
Ce23La6Y5Fe66B	34	17	0.64	0.16	0.2	0		7.41	5.03	X-Liao 2021 [43]

Table S5: magnetic properties of (Nd, Ce, La)-Fe-B melt spun ribbons (from [53]**)**

Composition (wt %)	Ce+R' wt%	Ce+R' at%	at. Ce/ (Ce+R')	at. La/ (Ce+R')	at. Nd/ (Ce+R')	Br T	[BH]max MGOe	Hc kOe
(Nd0.8Ce0.2)27Fe72B	27	12	0.2	0	0.8	0.86	14.5	8
(Nd0.8La0.2)27Fe72B	27	12	0	0.2	0.8	0.9	14.1	7.2
[Nd0.8(La0.4Ce0.6)0.2]27Fe72B	27	12	0.12	0.08	0.8	0.88	15.1	7.8
(Nd0.7Ce0.3)27Fe72B	27	12	0.3	0	0.7	0.85	12.6	7.6
(Nd0.8La0.3)27Fe72B	27	12	0	0.3	0.7	0.87	13.3	7.5
[Nd0.7(La0.4Ce0.6)0.3]27Fe72B	27	12	0.18	0.12	0.7	0.89	14.9	8
(Nd0.6Ce0.4)27Fe72B	27	12	0.4	0	0.6	0.81	11.3	6.7
(Nd0.6La0.4)27Fe72B	27	12	0	0.4	0.6	0.8	11.7	7.3
[Nd0.6(La0.4Ce0.6)0.4]27Fe72B	27	12	0.24	0.16	0.6	0.86	13.5	6.8
(Nd0.5Ce0.5)27Fe72B	27	12	0.5	0	0.5	0.73	8.2	6.2
(Nd0.5La0.5)27Fe72B	27	12	0	0.5	0.5	0.77	10.2	6.2
[Nd0.5(La0.4Ce0.6)0.5]27Fe72B	27	12	0.3	0.2	0.5	0.84	12.4	6.3

Table S6: magnetic properties of (Nd, Ce)-Fe-B hot-deformed magnets

Composition (wt %)	Infiltration phase (wt %)	Additive Elts (wt%)	Σ TR wt%	Σ TR at%	at. Ce/TR	at. (Nd+Pr)/TR	Br (T)	[BH]max [MGOe]	Hc (kOe)	Reference
(Nd0.8Ce0.2)30Fe59Co10B			30	14	0.2	0.8		31	9.4	Pathak 2015 [38]
Ce29.7Fe64.9Co4M0.41B0.9		M = Ga	30	13.8	1	0	0.63		0.25	Ito 2016 [58]
	Nd70Cu30 (10 %)		33.7	15.2	0.8	0.2	0.84		5.15	
		M = Ga	30	13.8	0.5	0.5			9.6	Ito 2016 [58]
	Nd70Cu30 (10 %)		34	16.3	0.4	0.6			17.1	
Nd22.8Ce7.4Fe64.5Co4M0.41B0.9		M = Ga	30.2	13.8	0.25	0.75			14.7	Ito 2016 [58]
	Nd70Cu30 (10 %)		34.2	16.2	0.2	0.8			20	
Ce29.8Fe64.72Co4.0M0.58B0.9		M = Cu (0.1) - Ga (0.4) - Al (0.08)	29.8	13.9	1	0	0.61		< 1	X-Tang 2018 [59]
	Nd70Cu30 (10 %)		33.8	16.3	0.8	0.2	0.96		5	
	Nd70Cu30 (40 %)		45.9	24.7	0.4	0.6	0.99		7	
Nd26.6Fe69.1M0.53B0.9		M = Ga	29.6	13.4	0	1	1.51		13.5	X-Tang 2019 [60]
Nd26.6Ce2.9Fe69.1M0.53B0.9		M = Ga	29.5	13.4	0.1	0.9	1.48		9.4	X-Tang 2019 [60]
Nd29.5Fe65Co4M0.53B0.9		M = Ga	29.5	13.4	0	1	1.49		13.6	X-Tang 2019 [60]
Nd26.6Ce2.9Fe65.1Co4M0.53B0.9		M = Ga	29.5	13.4	0.1	0.9	1.5		14.4	X-Tang 2019 [60]
Nd23.6Ce5.7Fe65.2Co4M0.53B0.9		M = Ga	29.5	13.4	0.2	0.8	1.48		12.6	X-Tang 2019 [60]
Nd20.7Ce8.6Fe65.2Co4M0.53B0.9		M = Ga	29.5	13.4	0.3	0.7	1.43		11.1	X-Tang 2019 [60]
Nd24Ce5.8Fe62.7Co6M0.64B0.9		M = Ga	29.8	13.6	0.2	0.8	0.9		10.8	Poenaru 2019 [57]
Nd21Ce8.7Fe62.8Co6M0.64B0.9		M = Ga	29.7	13.6	0.3	0.7	0.97		12	Poenaru 2019 [57]
Nd21.5Ce7Fe65.9Co4.1M0.57B0.9		M = Ga	28.5	12.9	0.25	0.75	1.37		14.4	X-Tang 2020 [61]
	Nd80Cu20 (12 %)		34.6	16.5	0.18	0.82	1.29		18.3	
Nd23.8Ce5.8Fe62.8Co6M0.64B0.9		M = Ga	29.6	13.5	0.2	0.8	1.37		14.4	X-Tang 2020 [61]
Nd25.1Ce6.1Fe61.5Co5.8M0.63B0.9		M = Ga	31.2	14.5	0.2	0.8	1.32	41.8	16.9	X-Tang 2020 [61]
Nd26.2Ce6.4Fe60.2Co5.7M0.61B0.9		M = Ga	32.6	15.5	0.2	0.8	1.2		16.9	X-Tang 2020 [61]

Table S7: Magnetic properties of sintered magnets SMP

Composition (wt %)	Additive elements M (wt/ %)	Σ Y,TR wt.%	Σ Y,TR at.%	at. Ce /TR	at. La/ TR	at. Y/ TR	at. Gd/ TR	at. Dy /TR	at. (Nd+Pr) /(Y+TR)	Br (T)	[BH]max [MGOe]	Hc (kOe)	Reference
(Nd, Pr)31.8Fe66.62M0.6B0.98	Al (0.15) - Cu (0.15) - Nb (0.3)	31.8	15	0	0	0	0	0	1	1.36	42.71	13.23	F-Chen 2022 [75]
(Nd, Pr)26.8Ce5Fe66.62M0.6B0.98	Al (0.15) - Cu (0.15) - Nb (0.3)	31.8	15	0.16	0	0	0	0	0.84	1.33	41.08	11.46	F-Chen 2022 [75]
(Nd, Pr)21.8Ce10Fe66.62M0.6B0.98	Al (0.15) - Cu (0.15) - Nb (0.3)	31.8	15	0.32	0	0	0	0	0.68	1.26	36.05	11.49	F-Chen 2022 [75]
(Nd, Pr)16.8Ce15Fe66.62M0.6B0.98	Al (0.15) - Cu (0.15) - Nb (0.3)	31.8	15	0.48	0	0	0	0	0.52	1.17	30.65	9.2	F-Chen 2022 [75]
Nd24.4Ce5.9Fe68.4M0.2B	Al (0.24) - Cu (0.1)	30.3	13.8	0.2	0	0	0	0	0.8	-	40.34	9.48	X-Fan 2022 [78]
Nd25Y3.9Fe69.9M0.2B	Al (0.24) - Cu (0.1)	28.9	13.8	0	0	0.2	0	0	0.8	-	43.15	11.73	X-Fan 2022 [78]
(Pr,Nd)27.5Dy3M0.2Fe68.3B	Al (0.1) - Cu (0.1)	27.5	13	0	0	0	0	0.08	0.92	1.323	43	19.21	C-Yan 2014a [72]
(Pr,Nd)25.3Ce2.2Dy3M0.2Fe68.3B	Al (0.1) - Cu (0.1)	27.5	13	0.08	0	0	0	0.08	0.85	1.307	41	16.72	C-Yan 2014a [72]
(Pr,Nd)23.1Ce4.4Dy3M0.2Fe68.3B	Al (0.1) - Cu (0.1)	27.5	13	0.15	0	0	0	0.08	0.77	1.292	40	14.99	C-Yan 2014a [72]
(Pr,Nd)20.9Ce6.6Dy3M0.2Fe68.3B	Al (0.1) - Cu (0.1)	27.5	13	0.23	0	0	0	0.08	0.69	1.244	36	16.72	C-Yan 2014a [72]
(Pr,Nd)18.7Ce8.8Dy3M0.2Fe68.3B	Al (0.1) - Cu (0.1)	27.5	13	0.31	0	0	0	0.08	0.62	1.208	34	15.78	C-Yan 2014a [72]
(Pr,Nd)12.1Ce15.4Dy3M0.2Fe68.3B	Al (0.1) - Cu (0.1)	27.5	13	0.54	0	0	0	0.08	0.38	1.133	26	11.33	C-Yan 2014a [72]
Nd22.9Ce7.6Fe68.3M0.2B	Al (0.1) - Cu (0.1)	30.5	13.9	0.25	0	0	0	0	0.75	1.312	39.86	11.82	X-Fan 2018 [77]
Nd22.9La7.6Fe68.3M0.2B	Al (0.1) - Cu (0.1)	30.5	13.9	0	0.25	0	0	0	0.75	1.248	35.52	6.19	X-Fan 2018 [77]
Nd22.9Y7.6Fe68.3M0.2B	Al (0.1) - Cu (0.1)	30.5	15.6	0	0	0.35	0	0	0.65	1.275	35.28	8.89	X-Fan 2018 [77]
(Nd,Pr)22.9Ce7.6Fe67.2M1.3B	Cu - Al - Ga - Zr	30.5	14	0.25	0	0	0	0	0.75	-	-	11.7	J-Jin 2019b [74]

Table S7: Magnetic properties of sintered magnets SMP (continued)

Composition (wt %)	Additive elements M (wt/ %)	Σ Y,TR wt.%	Σ Y,TR at.%	at. Ce /TR	at. La/ TR	at. Y/ TR	at. Gd/ TR	at. Dy /TR	at. (Nd+Pr) /(Y+TR)	Br (T)	[BH]max [MGOe]	Hc (kOe)	Reference
Nd28.8Pr3.2Fe66.5B	-	32.5		0	0	0	0	0	1	1.24	36	10	Okada 1985 [70]
(NdPr)31.8Ce1.6Fe65.5B	-	33.5		0.05	0	0	0	0	0.95	1.32	40	10.2	Okada 1985 [70]
(NdPr)20.1Ce12.8Fe65.5B	-	33.5		0.4	0	0	0	0	0.6	1.15	27	5.3	Okada 1985 [70]
Nd33.8Fe65B1.2	-	33.8	15.5	0	0	0	0	0	1	1.22	35	11	W-Tang 1989 [71]
Nd20.4La13.1Fe65.3B1.2	-	33.5	15.5	0	0.4	0	0	0	0.6	1.01	4	1	W-Tang 1989 [71]
Nd20.6La4.4Ce8.8Fe65.3B1.2	-	33.8	15.5	0.27	0.13	0	0	0	0.6	1.12	19	3.6	W-Tang 1989 [71]
Nd20.4La4.3Ce9Fe63.5M1.3B1.3	Al (1.3)	33.7	25.5	0.27	0.13	0	0	0	0.6	1.01	21	8.1	W-Tang 1989 [71]
Nd16Ce8Y5Fe69CoB	Cu - Al - Zr	29	14.4	0.25	0	0.25	0	0	0.5	1.38	44.6	6.7	Enokido 2021 [76]
Nd18Ce9Y5Fe67CoB	Cu - Al - Zr	32	16	0.25	0	0.25	0	0	0.5	1.27	36.2	11.56	Enokido 2021 [76]
Nd17Ce13Y2Fe66CoB	Cu - Al - Zr	32	16	0.4	0	0.1	0	0	0.5	1.22	32.7	13.35	Enokido 2021 [76]
Nd17Ce17Fe65CoB	Cu - Al - Zr	32	16	0.5	0	0	0	0	0.5	1.18	29.6	12.61	Enokido 2021 [76]
commercial magnets													
[(NdPrGd)0.5Ce0.5]30.5–31.5Febal.M1B N28	Al, Cu, Co, (Nb/Zr)	30.5-31.5		0.5				0	0.5		28	10.71	A-Li 2019 [99]
[(NdPrGd)0.65Ce0.35]30.5–31.5Febal. M1B N35	Al, Cu, Co, (Nb/Zr)	30.5-31.5		0.35				0	0.65		35	12.35	A-Li 2019 [99]
[(NdPrGd)0.7Ce0.3]30.5–31.5Febal.M1B N38M	Al, Cu, Co, (Nb/Zr)	30.5-31.5		0.3				0	0.7		38	14.72	A-Li 2019 [99]
[(NdPrGd)0.8Ce0.3]30.5–31.5Febal.M1B N38H	Al, Cu, Co, (Nb/Zr)	30.5-31.5		0.2				0	0.8		38	16.2	A-Li 2019 [99]

Table S8: Magnetic properties of sintered magnets SMP with MM

Composition (wt %)	MM /TR at%	Additive elts M (wt %)	Σ TR wt %	Σ TR at %	at. Ce /TR	at. La /TR	at. Dy /TR	at. (Nd+Pr) /TR	Br (T)	[BH]max [MGOe]	Hc (kOe)	Reference
Nd23.1Pr5.8Dy1.8Fe67M1.4B	0	Cu (0.1) - Al (0.1) – Nb (0.3)- Co (0.9)	30.6	13.9	0.00	0.00	0.05	0.95	1.33	42.42	16.93	E-Niu 2014 [82]
Nd21.3Pr5.4La0.9Ce1.7Dy1.6Fe66.9M1.3B	10.8	Cu (0.1) - Al (0.09) – Nb (0.27) - Co (0.86)	30.8	14.0	0.06	0.03	0.05	0.87	1.26	37.64	13.67	E-Niu 2014 [82]
Nd19.5Pr5La1.8Ce3.4Dy1.5Fe66.8M1.2B	21.5	Cu (0.09) - Al (0.08) – Nb (0.24) - Co (0.82)	31.0	14.2	0.11	0.06	0.04	0.79	1.21	34.04	10.70	E-Niu 2014 [82]
Nd16Pr4.1La3.5Ce6.7Dy1.1Fe66.6M1.1B	42.2	Cu (0.09) - Al (0.08) – Nb (0.18) - Co (0.74)	31.4	14.4	0.22	0.11	0.03	0.64	1.14	20.54	5.01	E-Niu 2014 [82]
Nd12.4Pr3.3La5.2Ce10.1Dy0.7Fe66.3M0.9B	62.1	Cu (0.08) - Al (0.04) – Nb (0.12) - Co (0.66)	31.8	14.7	0.32	0.17	0.02	0.49	1.09	13.77	2.75	E-Niu 2014 [82]
Nd8.9Pr2.5La7Ce13.4Dy0.4Fe66.1M0.7B	81.4	Cu (0.08) - Al (0.02) – Nb (0.06) - Co (0.58)	32.1	15.0	0.42	0.22	0.01	0.35	1.06	8.91	1.23	E-Niu 2014 [82]
Nd5.4Pr1.7La8.7Ce16.7DyFe65.9M0.6B	100	Cu (0.08) - Co (0.5)	32.5	15.3	0.52	0.27	0	0.21	0.95	2.40	0.46	E-Niu 2014 [82]
Nd21.3Pr0.2La2.5Ce4.8Fe69.8M0.51B0.96	30	Cu (0.1) - Al (0.11) – Nb (0.3)	28.7	12.9	0.17	0.09	0	0.75	1.31	37.8	7.6	X-Yu 2018 [85]
Nd4.6Pr1.5La7.7Ce16.9Fe66.2M2B0.96	100	Cu (0.15) - Al (0.3) – Zr (0.22) - Ga (0.35) - Co (1)	30.8	14.3	0.55	0.25	0	0.20	0.957	8.05	1.41	W-Liu 2019 [86]
GBDP (0.5 % TbHx)									0.928	20.2	6.81	

Table S9: Magnetic properties of sintered magnets with MMP

Composition (wt %)	Additive elts M (wt.%)	Σ TR wt %	Σ TR at %	at. Ce /TR	at. La /TR	at. Y /TR	at. Gd /TR	at. (Nd+Pr) /TR	Br (T)	[BH]max [MGOe]	Hc (kOe)	Reference
Nd27Ce3(FeTM)69B	not given	30	13.5	0.1	0	0	0	0.9	1.4	46.6	12.2	M-Zhu 2014 [87]
Nd22.5Ce4.5(FeTM)69B	not given	30	13.5	0.15	0	0	0	0.85	1.38	45.6	11.4	M-Zhu 2014 [87]
Nd24Ce6(FeTM)69B	not given	30	13.5	0.2	0	0	0	0.8	1.37	45	12	M-Zhu 2014 [87]
Nd21Ce9(FeTM)69B	not given	30	13.5	0.3	0	0	0	0.7	1.36	43.3	9.26	M-Zhu 2014 [87]
Nd26.5Ce13.5(FeTM)69B	not given	30	13.5	0.45	0	0	0	0.55	1.24	33.4	6.2	M-Zhu 2014 [87]
(Nd,Pr)24.8Ce6.2Fe67.1M0.9B (SMP) (Nd,Pr)24.8Ce6.2Fe67.1M0.9B	not given	31 31	14.1 14.1	0.2 0.2	0 0	0 0	0 0	0.8 0.8	1.316 1.33		7.7 12.1	M-Zhu 2015 [91]
Nd25.5Ce4.5Fe68.9M0.1B	Cu	30	13.6	0.15	0	0	0	0.85	1.38	45.2	11.9	S-Huang 2015 [89]
Nd22.9Cu7.6Fe68.3M0.2B (SMP) Nd22.9Cu7.6Fe68.3M0.2B	Al (0.1) - Cu (0.1)	30.5 30.5	14 14	0.25 0.25	0 0	0 0	0 0	0.75 0.75	1.307 1.33	39.44 40.5	10.26 12.14	X-Fan 2016 [92]
(PrNd)29.8Gd1.7Fe66.4M1.1B	Cu, Al, Nb, Zr	31.5	14.3	0.00	0	0	0.05	0.95	1.3	41.9	14.4	J-Jin 2016a [15]
La0.98Ce1.82(PrNd)27Gd1.7Fe66.4M1.1B	Cu, Al, Nb, Zr	31.5	14.2	0.06	0.03	0	0.05	0.86	1.29		13.7	J-Jin 2016a [15]
La2Ce3.71(PrNd)24.1Gd1.7Fe66.4M1.1B	Cu, Al, Nb, Zr	31.5	14.3	0.12	0.06	0	0.05	0.77	1.27	39.7	12.2	J-Jin 2016a [15]
La2.98Ce5.53(PrNd)27Gd21.3Fe66.4M1.1B	Cu, Al, Nb, Zr	31.5	14.4	0.18	0.10	0	0.05	0.67	1.25		10.1	J-Jin 2016a [15]
La4Ce7.41(PrNd)18.4Gd1.7Fe66.4M1.1B	Cu, Al, Nb, Zr	31.5	14.5	0.24	0.13	0	0.05	0.58	1.22		8.9	J-Jin 2016a [15]
(Pr,Nd)30.5Fe67.5M1B	Al, Cu, Ga, Zr	30.5	13.9	0	0	0	0	1.00	1.38	48.7	13.8	Y-Peng [27]
(Pr,Nd)22.27Ce8.24Fe67.5M1B (SMP) (Pr,Nd)22.27Ce8.24Fe67.5M1B	Al, Cu, Ga, Zr	30.5 30.5	13.9 13.9	0.27 0.27	0 0	0 0	0 0	0.73 0.73	1.28 1.3	39 41.1	10.40 11.40	Y-Zhang 2017a [27]
(Pr,Nd)19.52Ce10.98Fe67.5M1B	Al, Cu, Ga, Zr	30.5	13.9	0.36	0	0	0	0.64	1.27	38.8	10.30	Y-Zhang 2017a [27]
(Pr,Nd)16.78Ce13.73Fe67.5M1B	Al, Cu, Ga, Zr	30.5	14	0.45	0	0	0	0.55	1.24	36.7	9.00	Y-Zhang 2017a [27]
(Pr,Nd)30.5Fe67.2M1.3B	Al, Cu, Ga, Zr	30.5	14	0	0	0	0	1	1.39	47.6	14.90	B-Peng 2017 [106]
(Nd+Pr)24.5Ce3.9Y2.1Fe67.2M1.3B	Al, Cu, Ga, Zr	30.5	14.3	0.13	0	0.1	0	0.77	1.38		12.6	B-Peng 2017 [106]
(Nd+Pr)21.5Ce5.85Y3.15Fe67.2M1.3B	Al, Cu, Ga, Zr	30.5	14.7	0.18	0	0.16	0	0.66	1.37	45.6	11.8	B-Peng 2017 [106]
(Nd+Pr)18.5Ce7.8Y4.2Fe67.2M1.3B	Al, Cu, Ga, Zr	30.5	15	0.24	0	0.21	0	0.55	1.35	43.9	11.1	B-Peng 2017 [106]
(Nd+Pr)21.5Ce9Fe67.2M1.3B	Al, Cu, Ga, Zr	30.5	13.9	0.3	0	0	0	0.7	1.35	43.9	11.1	B-Peng 2017 [106]
Nd18.5Ce9.9La2.5Fe66.3M1.9B0.96	Al, Cu, Ga, Co, Zr	30.8	14.2	0.32	0.08	0	0	0.6	1.271	39.39	7.27	H-Chen 2022a [104]
Nd20.4Ce10.9La2.7Fe63.7M1.43B0.92	Al, Cu, Ga, Co, Zr	33.9	16	0.32	0.08	0	0	0.6	1.212	35.58	11.1	H-Chen 2022a [104]

Table S9: Magnetic properties of sintered magnets with MMP (continued)

Composition (wt %)	Additive elts M (wt.%)	Σ TR wt %	Σ TR at %	at. Ce /TR	at. La /TR	at. Y /TR	at. Gd /TR	at. (Nd+Pr) /TR	Br (T)	[BH]max [MGOe]	Hc (kOe)	Reference
(Pr,Nd)29.8Gd1.7Fe66.4M1.1B	Cu, Al, Nb, Zr	30.5	14.3	0	0	0	0.05	0.95	1.3	41.96	14.43	J-Jin 2018b [100]
(Pr,Nd)27.0La0.98Ce1.82Gd1.7Fe66.4M1.1(SMP)	Cu, Al, Nb, Zr	30.5	14.4	0.06	0.03	0	0.05	0.86	1.27	38.44	9.82	J-Jin 2018b [100]
(Pr,Nd)27.0La0.98Ce1.82Gd1.7Fe66.4M1.1B		30.5	14.4	0.06	0.03	0	0.05	0.86	1.29	41.46	13.93	
(Pr,Nd)27.0La2Ce3.7Gd1.7Fe66.4M1.1B	Cu, Al, Nb, Zr	30.5	14.3	0.12	0.06	0	0.05	0.77	1.28	40.33	12.83	J-Jin 2018b [100]
(Nd,Pr)16.8Ce13.7Fe67.5M1.0B1.0	Cu	30.5	14	0.46	0	0	0	0.54	1.21	33.7	9.1	Y-Zhang 2018a [97]
(Nd,Pr)31.3Fe66.7M1.0B0.98	Cu	31.3	14.3	0	0	0	0	1	1.28		13.8	Y-Zhang 2019c [94]
(Nd,Pr)28.5Ce2.8Fe66.7M1.0B0.98	Cu	31.3	14.3	0.09	0	0	0	0.91	1.28		12.1	Y-Zhang 2019c [94]
(Nd,Pr)25.7Ce5.8Fe66.7M1.0B0.98	Cu	31.3	14.4	0.18	0	0	0	0.82	1.26		11.8	Y-Zhang 2019c [94]
(Pr,Nd)22.8Ce10.7Fe64.8M0.66B0.97	Al, Cu, Zr	33.5	15.7	0.32	0	0	0	0.68	1.149	28.7	6.5	Q-Shi 2019 [101]
(Pr,Nd)22.8Ce6.95La3.74Fe64.8M0.66B	Al, Cu, Zr	33.5	15.7	0.21	0.11	0	0	0.68	1.238	34.7	6.16	Q-Shi 2019 [101]
(Nd,Pr)21.3Ce5.5La3Gd1.7Fe66.4M1.1B	Cu, Al, Nb ,Zr	31.5	14.4	0.18	0.2	0	0.05	0.57	1.25	38.2	10.4	J-Jin 2020a [102]
(Pr,Nd)22.88Ce4.96La2.67Fe67.1M1.4B	Cu, Al, Ga, Zr	30.5	13.9	0.17	0.09	0	0	0.84	1.31	41.67	13	J-Jin 2019a [98]
Nd12.87Pr9.66Ce5.95La3.03Fe65.5M2B	Al, Cu, Ga, Co, Zr	31.5	14.6	0.19	0.1	0	0	0.71	1.245	38.21	11.03	H-Chen 2020b [105]
(Pr,Nd)24.8Ce6.2(Fe,TM)68B (SMP)	not given	31	14.2	0.2	0	0	0	0.8	1.33	40.2	10.4	R-Han 2020 [93]
(Pr,Nd)24.8Ce6.2(Fe,TM)68B		31	14.2	0.2	0	0	0	0.8	1.34	41.9	12.7	
(Pr,Nd)22.52Ce7.39Fe67.9M1.18B	Al, Cu, Ga,Nb	29.9	13.6	0.25	0	0	0	0.75	1.29	37.8	6.9	Z-Wei 2020 [103]
(Pr,Nd)22.5Ce4.8La2.6Fe68M1.18B	Al, Cu, Ga,Nb	29.9	13.6	0.16	0.09	0	0	0.75	1.3	39.5	8.8	Z-Wei 2020 [103]
Nd5.6Pr2Ce20.7La0.7Y1.5Gd2.6Fe64M1.9B1.1	Co, Al, Cu, Zr	33.1	15.7	0.62	0.02	0.07	0.07	0.22	0.92	20.17	5.57	A-Li 2020a [67]
Nd24.8Ce6.2Fe67.1M0.9B (SMP)	Co, Al, Cu, Nb, Ga	31	14.2	0.2	0	0	0	0.8	1.323	40.54	11.91	H-Chen 2020c [95]
Nd24.8Ce6.2Fe67.1M0.9B	Co, Al, Cu, Nb, Ga	31	14.2	0.2	0	0	0	0.8	1.325	40.4	12.66	
(NdPr)27.76Ce1.78La0.96Fe67.1M1.4B	Al, Cu, Ga, Zr	30.5	13.9	0.06	0.04	0	0	0.9	1.4	47.9	13	D-Liu 2022 [107]
(NdPr)19.52Ce7.14La3.84Fe67.1M1.4B	Al, Cu, Ga, Zr	30.4	13.9	0.24	0.13	0	0	0.63	1.34	42.2	9.6	D-Liu 2022 [107]

Table S10: Magnetic properties of sintered magnets by SPS

Composition (wt %)	Additive elts in alloy M (w%) Compound used in GBR (wt%)	Σ TR wt%	Σ TR at%	at. Ce /TR	at. Dy /TR	at. (Nd+Pr) /TR	Br (T)	[BH]max [MGOe]	Hc (kOe)	Δ NM (*)	Δ Hc (kOe)	Reference
Ce35Fe61Co1.72M1.4B	M: Nb, Cu, Ga	35	17	1.00	0	0.00	0.37	2	2.75			Q-Jiang 2019 [138]
	Nd80Cu20 (20 %)	45.0	23	0.63	0	0.37	0.47	3.77	5.98	5.00	3.23	
Nd16.9Pr1.05Ce11.8Fe67M2.2B (50% MQU-F - 50% MQP)	M: Co, Ga	29.8	13.60	0.40	0	0.60	0.75	12.09	13.20			XG-Cui 2020 [135]
	Pr68Cu32 (1%)	30.1	13.80	0.39	0	0.61	0.74	11.70	13.69	0.10	0.49	
	Pr68Cu32 (2%)	30.5	14.00	0.39	0	0.61	0.74	11.58	14.20	0.49	1.00	
	Pr68Cu32 (3%)	31.3	14.40	0.37	0	0.63	0.72	10.95	15.01	0.68	1.81	
50% MQU-F - 50% MQP		29.7		*0.64*	*0.00*	*0.36*	0.73	9.9	7.54			XG-Cui 2022 [137]
	DyF3-Cu (1%)	30.8		*0.58*	*0.06*	*0.36*	0.73	10.1	7.85	0.46	0.31	
	DyF3-Cu (2%)	31.6		*0.52*	*0.09*	*0.40*	0.70	10.2	12.31	4.56	4.46	
	DyF3-Cu (3%)	34.9		*0.48*	*0.13*	*0.39*	0.67	9.6	14.07	5.79	6.22	
Nd15Pr4.9Ce4.9Fz72.5M1.6B1.1 (MQP-13-9HD)	M: Zr	24.8	10.9	0.20	0	0.80	0.68	9.55	8.22			L-He 2021 [136]
	Pr30Fe69B (25%)	26.1	11.6	0.15	0	0.85	0.76	10.80	8.51	1.55	0.29	
	Pr30Fe69B (50 %)	27.4	12.3	0.09	0	0.91	0.79	11.56	9.40	3.19	1.18	
	Pr30Fe69B (75%)	28.7	13.1	0.05	0	0.95	0.80	13.07	10.87	6.17	2.65	
Pr30Fe69B		30.0	13.8	0.00	0	1.00	0.78	12.56	11.55	6.34	3.33	

References

[1] H. Sepehri-Amin, S. Hirosawa, and K. Hono, “Chapter 4 - Advances in Nd-Fe-B Based Permanent Magnets,” in *Handbook of Magnetic Materials*, E. Brück, Ed., Elsevier, 2018, pp. 269–372. [Online]. Available: https://www.sciencedirect.com/science/article/pii/S1567271918300039

[2] O. Gutfleisch, M. A. Willard, E. Brück, C. H. Chen, S. G. Sankar, and J. P. Liu, “Magnetic materials and devices for the 21st century: Stronger, lighter, and more energy efficient,” *Adv. Mater.*, vol. 23, no. 7, pp. 821–842, 2011, doi: 10.1002/adma.201002180.

[3] R. Gauß and Carlo Burkhardt, “Rare Earth Magnets and Motors: A European Call for Action. A report by the Rare Earth Magnets and Motors Cluster of the European Raw Materials Alliance. Berlin 2021,” Berlin, 2021.

[4] J. Cui *et al.*, “Current progress and future challenges in rare-earth-free permanent magnets,” *Acta Mater.*, vol. 158, pp. 118–137, 2018, doi: 10.1016/j.actamat.2018.07.049.

[5] K. Hono and H. Sepehri-Amin, “Prospect for HRE-free high coercivity Nd-Fe-B permanent magnets,” *Scr. Mater.*, vol. 151, pp. 6–13, Jul. 2018, doi: 10.1016/j.scriptamat.2018.03.012.

[6] A. K. Pathak, K. A. Gschneidner, M. Khan, R. W. McCallum, and V. K. Pecharsky, “High performance Nd-Fe-B permanent magnets without critical elements,” *J. Alloys Compd.*, vol. 668, pp. 80–86, May 2016, doi: 10.1016/j.jallcom.2016.01.194.

[7] A. Li *et al.*, “Development of Ce-based sintered magnets: review and prospect,” *J. Iron Steel Res. Int.*, vol. 27, no. 1, pp. 1–11, Jan. 2020, doi: 10.1007/s42243-019-00287-x.

[8] Z. C. Sims *et al.*, “How Cerium and Lanthanum as Coproducts Promote Stable Rare Earth Production and New Alloys,” *J. Sustain. Metall.*, vol. 8, no. 3, pp. 1225–1234, Sep. 2022, doi: 10.1007/s40831-022-00562-4.

[9] S. Dong, W. Li, H. Chen, and R. Han, “The status of Chinese permanent magnet industry and R&D activities,” *AIP Adv.*, vol. 7, no. 5, p. 056237, Mar. 2017, doi: 10.1063/1.4978699.

[10] X. Rao, E. Niu, and B. Hu, “Effects of cerium on permanent magnetic properties of sintered Nd-Fe-B magnets,” *Mater. China*, vol. 36, no. 1, pp. 63–74, 2017, doi: 10.7502/j.issn.1674-3962.2017.01.09.

[11] Q. Jiang and Z. Zhong, “Research and development of Ce-containing Nd2Fe14B-type alloys and permanent magnetic materials,” *J. Mater. Sci. Technol.*, vol. 33, no. 10, pp. 1087–1096, Oct. 2017, doi: 10.1016/j.jmst.2017.06.019.

[12] J. F. Herbst, “RE2FE14B materials: Intrinsic properties and technological aspects,” *Rev. Mod. Phys.*, vol. 63, no. 4, pp. 819–898, Oct. 1991, doi: 10.1103/RevModPhys.63.819.

[13] C. V. Colin, M. Ito, M. Yano, N. M. Dempsey, E. Suard, and D. Givord, “Solid-solution stability and preferential site-occupancy in (R-R′)2Fe14B compounds,” *Appl. Phys. Lett.*, vol. 108, no. 24, p. 242415, Jun. 2016, doi: 10.1063/1.4953874.

[14] J. Boust *et al.*, “Ce and Dy substitutions in Nd2 Fe14 B: Site-specific magnetic anisotropy from first principles,” *Phys. Rev. Mater.*, vol. 6, no. 8, 2022, doi: 10.1103/PhysRevMaterials.6.084410.

[15] J. Jin, Y. Zhang, T. Ma, and M. Yan, “Mechanical Properties of La–Ce-Substituted Nd–Fe–B Magnets,” *IEEE Trans. Magn.*, vol. 52, no. 7, pp. 1–4, Jul. 2016, doi: 10.1109/TMAG.2016.2524019.

[16] T. W. Capehart, R. K. Mishra, G. P. Meisner, C. D. Fuerst, and J. F. Herbst, “Steric variation of the cerium valence in Ce2Fe14B and related compounds,” *Appl. Phys. Lett.*, vol. 63, no. 26, pp. 3642–3644, Dec. 1993, doi: 10.1063/1.110075.

[17] A. Alam, M. Khan, R. W. McCallum, and D. D. Johnson, “Site-preference and valency for rare-earth sites in (R-Ce)2Fe14B magnets,” *Appl. Phys. Lett.*, vol. 102, no. 4, p. 042402, Jan. 2013, doi: 10.1063/1.4789527.
[18] Z. B. Li, B. G. Shen, M. Zhang, F. X. Hu, and J. R. Sun, “Substitution of Ce for Nd in preparing R2Fe14B nanocrystalline magnets,” *J. Alloys Compd.*, vol. 628, pp. 325–328, Apr. 2015, doi: 10.1016/j.jallcom.2014.12.042.
[19] Z. Li *et al.*, “Effects of CE substitution on the microstructures and intrinsic magnetic properties of Nd–Fe–B alloy,” *J. Magn. Magn. Mater.*, vol. 393, pp. 551–554, Nov. 2015, doi: 10.1016/j.jmmm.2015.06.028.
[20] J. Sugiyama *et al.*, “Magnetic moment of rare earth elements in R2Fe14B estimated with μ+SR,” *Phys. Rev. Mater.*, vol. 3, no. 6, p. 064402, Jun. 2019, doi: 10.1103/PhysRevMaterials.3.064402.
[21] A. Alam and D. D. Johnson, “Mixed valency and site-preference chemistry for cerium and its compounds: A predictive density-functional theory study,” *Phys. Rev. B*, vol. 89, no. 23, p. 235126, Jun. 2014, doi: 10.1103/PhysRevB.89.235126.
[22] J. Jin *et al.*, “Manipulating Ce Valence in RE2Fe14B Tetragonal Compounds by La-Ce Co-doping: Resultant Crystallographic and Magnetic Anomaly,” *Sci. Rep.*, vol. 6, no. 1, p. 30194, Jul. 2016, doi: 10.1038/srep30194.
[23] K. Xu *et al.*, “Experimental and computational study on the phase formation and magnetic properties of Ce-La-Fe-B alloys,” *J. Magn. Magn. Mater.*, vol. 461, pp. 100–105, Sep. 2018, doi: 10.1016/j.jmmm.2018.04.058.
[24] X. Tan, H. Li, H. Xu, K. Han, W. Li, and F. Zhang, “A Cost-Effective Approach to Optimizing Microstructure and Magnetic Properties in Ce17Fe78B6 Alloys,” *Materials*, vol. 10, no. 8, 2017, doi: 10.3390/ma10080869.
[25] J. J. Croat, J. F. Herbst, R. W. Lee, and F. E. Pinkerton, “Pr-Fe and Nd-Fe-based materials: A new class of high-performance permanent magnets (invited),” *J. Appl. Phys.*, vol. 55, no. 6, pp. 2078–2082, Mar. 1984, doi: 10.1063/1.333571.
[26] J. F. Herbst, M. S. Meyer, and F. E. Pinkerton, “Magnetic hardening of Ce2Fe14B,” *J. Appl. Phys.*, vol. 111, no. 7, p. 07A718, Feb. 2012, doi: 10.1063/1.3675175.
[27] Y. Zhang *et al.*, “Effects of REFe2 on microstructure and magnetic properties of Nd-Ce-Fe-B sintered magnets,” *Acta Mater.*, vol. 128, pp. 22–30, Apr. 2017, doi: 10.1016/j.actamat.2017.02.002.
[28] Z. Li, M. Zhang, B. Shen, F. Hu, and J. Sun, “Variations of phase constitution and magnetic properties with Ce content in Ce-Fe-B permanent magnets,” *Mater. Lett.*, vol. 172, pp. 102–104, Jun. 2016, doi: 10.1016/j.matlet.2016.02.149.
[29] M. Grigoras, M. Lostun, G. Stoian, D. D. Herea, H. Chiriac, and N. Lupu, “Microstructure and magnetic properties of Ce10+xFe84−xB6 nanocrystalline ribbons versus preparation conditions,” *J. Magn. Magn. Mater.*, vol. 432, pp. 119–123, Jun. 2017, doi: 10.1016/j.jmmm.2017.01.062.
[30] Q. Y. Zhou, Z. Liu, S. Guo, A. R. Yan, and D. Lee, “Magnetic Properties and Microstructure of Melt-Spun Ce–Fe–B Magnets,” *IEEE Trans. Magn.*, vol. 51, no. 11, pp. 1–4, Nov. 2015, doi: 10.1109/TMAG.2015.2447553.
[31] L. Z. Zhao *et al.*, “Structure, magnetic properties and Mössbauer study of melt-spun nanocrystalline Ce-rich ternary Ce-Fe-B alloy,” *J. Alloys Compd.*, vol. 715, pp. 60–64, Aug. 2017, doi: 10.1016/j.jallcom.2017.04.320.
[32] W. Cui *et al.*, “Enhanced coercivity and grain boundary chemistry in diffusion-processed Ce13Fe79B8 ribbons,” *Mater. Lett.*, vol. 191, pp. 210–213, Mar. 2017, doi: 10.1016/j.matlet.2016.12.060.

[33] Z. LI *et al.*, “Effects of lanthanum substitution on microstructures and intrinsic magnetic properties of Nd-Fe-B alloy,” *J. Rare Earths*, vol. 33, no. 9, pp. 961–964, Sep. 2015, doi: 10.1016/S1002-0721(14)60512-3.
[34] Q. Zhou, R. Tang, F. Xiao, and Z. Liu, “Coercivity Enhancement of Nd–Ce–Fe–B Sintered Magnets by the Grain Boundary Diffusion Process Using Nd–Al–Cu Alloy,” *IEEE Trans. Magn.*, vol. 54, no. 11, pp. 1–4, Nov. 2018, doi: 10.1109/TMAG.2018.2835841.
[35] L. Z. Zhao, J. S. Zhang, G. Ahmed, X. F. Liao, Z. W. Liu, and J. M. Greneche, “Understanding the element segregation and phase separation in the Ce-substituted Nd-(Fe,Co)-B based alloys,” *Sci. Rep.*, vol. 8, no. 1, p. 6826, May 2018, doi: 10.1038/s41598-018-25230-0.
[36] T. D. Hien, L. T. Tai, R. Grössinger, R. Krewenka, F. R. de Boer, and F. F. Bekker, “Comparison of the magnetic properties of MM-Fe-B and Nd-Fe-B compounds,” *J. Common Met.*, vol. 127, pp. 111–116, Jan. 1987, doi: 10.1016/0022-5088(87)90366-3.
[37] A. K. Pathak *et al.*, “Magnetic properties of bulk, and rapidly solidified nanostructured (Nd1-xCex)2Fe14-yCoyB ribbons,” *Acta Mater.*, vol. 103, pp. 211–216, Jan. 2016, doi: 10.1016/j.actamat.2015.09.049.
[38] A. K. Pathak *et al.*, “Cerium: An Unlikely Replacement of Dysprosium in High Performance Nd–Fe–B Permanent Magnets,” *Adv. Mater.*, vol. 27, no. 16, pp. 2663–2667, Apr. 2015, doi: 10.1002/adma.201404892.
[39] R. Q. Wang, Y. Liu, J. Li, W. Zhao, and X. J. Yang, “Mössbauer and TEM studies of the phase composition and structure of (Nd1−xCex)32.7Fe66.22B1.08 ribbons,” *J. Mater. Sci.*, vol. 52, no. 12, pp. 7311–7322, Jun. 2017, doi: 10.1007/s10853-017-0967-z.
[40] M. Yang, H. Wang, Y. Hu, L. Yang, A. Maclennan, and B. Yang, “Increased coercivity for Nd-Fe-B melt spun ribbons with 20 at.% Ce addition: The role of compositional fluctuation and Ce valence state,” *J. Alloys Compd.*, vol. 710, pp. 519–527, Jul. 2017, doi: 10.1016/j.jallcom.2017.03.305.
[41] M. Zhang, W. Zhang, F. Chen, Y. Guo, F. Li, and W. Liu, “Effect of Heat Treatment on Microstructure and Magnetic Properties of Ce-Doped NdFeB Ribbons,” *J. Supercond. Nov. Magn.*, vol. 31, no. 9, pp. 2811–2816, Sep. 2018, doi: 10.1007/s10948-017-4553-z.
[42] M. H. Rong *et al.*, “Phase Structure, Microstructure, and Magnetic Properties of (Nd-Ce)13.4Fe79.9B6.7 Alloys,” *J. Supercond. Nov. Magn.*, vol. 33, no. 9, pp. 2737–2744, Sep. 2020, doi: 10.1007/s10948-020-05537-8.
[43] X. Liao *et al.*, “Development of cost-effective nanocrystalline multi-component (Ce,La,Y)-Fe-B permanent magnetic alloys containing no critical rare earth elements of Dy, Tb, Pr and Nd,” *J. Mater. Sci. Technol.*, vol. 76, pp. 215–221, Jun. 2021, doi: 10.1016/j.jmst.2020.11.027.
[44] Z. Li *et al.*, “Gd substitution for Ce in preparing (Ce,Gd)-Fe-B magnets,” *J. Alloys Compd.*, vol. 729, pp. 988–991, Dec. 2017, doi: 10.1016/j.jallcom.2017.09.243.
[45] D. N. Brown, D. Lau, and Z. Chen, “Substitution of Nd with other rare earth elements in melt spun Nd2Fe14B magnets,” *AIP Adv.*, vol. 6, no. 5, p. 056019, Mar. 2016, doi: 10.1063/1.4944080.
[46] Z. Li *et al.*, “Tuning the structure and intrinsic magnetic properties of Ce2Fe14B alloys by elimination of CeFe2 with La substitution,” *J. Magn. Magn. Mater.*, vol. 505, p. 166747, Jul. 2020, doi: 10.1016/j.jmmm.2020.166747.
[47] X. F. Liao *et al.*, “Maximizing the hard magnetic properties of melt-spun Ce–La–Fe–B alloys,” *J. Mater. Sci.*, vol. 54, no. 9, pp. 7288–7299, May 2019, doi: 10.1007/s10853-019-03387-x.

[48] X. F. Liao *et al.*, “Clarifying the basic phase structure and magnetic behavior of directly quenched (Ce,La)2Fe14B alloys with various Ce/La ratios,” *Curr. Appl. Phys.*, vol. 19, no. 6, pp. 733–738, Jun. 2019, doi: 10.1016/j.cap.2019.04.002.
[49] Z. CHEN, J. LUO, Y. SUI, and Z. GUO, “Effect of yttrium substitution on magnetic properties and microstructure of Nd-Y-Fe-B nanocomposite magnets,” *J. Rare Earths*, vol. 28, no. 2, pp. 277–281, Apr. 2010, doi: 10.1016/S1002-0721(09)60096-X.
[50] X. Liao *et al.*, “Exceptional elevated temperature behavior of nanocrystalline stoichiometric Y2Fe14B alloys with La or Ce substitutions,” *J. Mater. Sci.*, vol. 54, no. 23, pp. 14577–14587, Dec. 2019, doi: 10.1007/s10853-019-03916-8.
[51] L.-J. Liu and Z. Liu, “Effect of annealing technology on coercivity and thermal stability in (CePrNd)-Fe-B sintered magnet,” *Zhongguo Youse Jinshu XuebaoChinese J. Nonferrous Met.*, vol. 29, no. 12, pp. 2785–2792, 2019, doi: 10.19476/j.ysxb.1004.0609.2019.12.11.
[52] Y. Liu, J. Jin, T. Ma, B. Peng, X. Wang, and M. Yan, “Promoting the La solution in 2:14:1-type compound: Resultant chemical deviation and microstructural nanoheterogeneity,” *J. Mater. Sci. Technol.*, vol. 62, pp. 195–202, Jan. 2021, doi: 10.1016/j.jmst.2020.06.009.
[53] X. Lin *et al.*, “Phase structure evolution and magnetic properties of La/Ce doped melt-spun NdFeB alloys,” *J. Magn. Magn. Mater.*, vol. 490, p. 165454, Nov. 2019, doi: 10.1016/j.jmmm.2019.165454.
[54] R. W. Lee, “Hot-pressed neodymium-iron-boron magnets,” *Appl. Phys. Lett.*, vol. 46, no. 8, pp. 790–791, 1985, doi: 10.1063/1.95884.
[55] Y. Yoshida, N. Yoshikawa, T. Nishio, Y. Kasai, V. Panchanathan, and J. J. Croat, “Effect of additives on hot deformation behavior of melt-spun Nd-Fe-Co-B magnets,” *J. Appl. Phys.*, vol. 70, no. 10, pp. 6363–6365, Nov. 1991, doi: 10.1063/1.349943.
[56] K. Y. Ko, S. Yoon, J. G. Booth, Al-kanani H. J., and S. K. Cho, “Magnetic properties and microstructures of mischmetal-FeB-(Al, Ti and Al-Co) permanent magnets,” *J. Mater. Sci.*, vol. 37, no. 7, pp. 1421–1427, Apr. 2002, doi: 10.1023/A:1014593217529.
[57] I. Poenaru *et al.*, “Ce and La as substitutes for Nd in Nd2Fe14B-based melt-spun alloys and hot-deformed magnets: a comparison of structural and magnetic properties,” *J. Magn. Magn. Mater.*, vol. 478, pp. 198–205, May 2019, doi: 10.1016/j.jmmm.2019.01.095.
[58] M. Ito *et al.*, “Coercivity enhancement in Ce-Fe-B based magnets by core-shell grain structuring,” *AIP Adv.*, vol. 6, no. 5, p. 056029, Mar. 2016, doi: 10.1063/1.4945040.
[59] X. Tang *et al.*, “Coercivity enhancement of hot-deformed Ce-Fe-B magnets by grain boundary infiltration of Nd-Cu eutectic alloy,” *Acta Mater.*, vol. 144, pp. 884–895, Feb. 2018, doi: 10.1016/j.actamat.2017.10.071.
[60] X. Tang, H. Sepehri-Amin, M. Matsumoto, T. Ohkubo, and K. Hono, “Role of Co on the magnetic properties of Ce-substituted Nd-Fe-B hot-deformed magnets,” *Acta Mater.*, vol. 175, pp. 1–10, Aug. 2019, doi: 10.1016/j.actamat.2019.05.064.
[61] X. Tang, S. Y. Song, J. Li, H. Sepehri-Amin, T. Ohkubo, and K. Hono, “Thermally-stable high coercivity Ce-substituted hot-deformed magnets with 20% Nd reduction,” *Acta Mater.*, vol. 190, pp. 8–15, May 2020, doi: 10.1016/j.actamat.2020.03.017.
[62] Y. Kaneko, F. Kuniyoshi, and N. Ishigaki, “Proven technologies on high-performance Nd–Fe–B sintered magnets,” *Proc. Rare Earths04 Nara Jpn.*, vol. 408–412, pp. 1344–1349, Feb. 2006, doi: 10.1016/j.jallcom.2005.04.169.
[63] J. Bernardi, J. Fidler, M. Sagawa, and Y. Hirose, “Microstructural analysis of strip cast Nd–Fe–B alloys for high (BH)max magnets,” *J. Appl. Phys.*, vol. 83, no. 11, pp. 6396–6398, Jun. 1998, doi: 10.1063/1.367557.

[64] C. Yan, S. Guo, R. Chen, D. Lee, and A. Yan, “Enhanced Magnetic Properties of Sintered Ce–Fe–B-Based Magnets by Optimizing the Microstructure of Strip-Casting Alloys,” *IEEE Trans. Magn.*, vol. 50, no. 11, pp. 1–4, Nov. 2014, doi: 10.1109/TMAG.2014.2325404.
[65] C.-J. Yan, S. Guo, R.-J. Chen, D. Lee, and A.-R. Yan, “Phase constitution and microstructure of Ce—Fe—B strip-casting alloy,” *Chin. Phys. B*, vol. 23, no. 10, p. 107501, Oct. 2014, doi: 10.1088/1674-1056/23/10/107501.
[66] J. Jin *et al.*, “Novel hydrogen decrepitation behaviors of (La, Ce)-Fe-B strips,” *AIP Adv.*, vol. 8, no. 5, p. 056233, Jan. 2018, doi: 10.1063/1.5006432.
[67] A. Li, W. Yang, H. Feng, X. Chen, M. Zhu, and W. Li, “Novel PrNd-Lean Ce-Based $R_2Fe_{14}B$ Permanent Magnets With High Performance,” *IEEE Trans. Magn.*, vol. 56, no. 10, pp. 1–5, 2020, doi: 10.1109/TMAG.2020.3015203.
[68] I. Poenaru *et al.*, “HDDR treatment of Ce-substituted Nd2Fe14B-based permanent magnet alloys - phase structure evolution, intergranular processes and magnetic property development,” *J. Alloys Compd.*, vol. 814, p. 152215, Jan. 2020, doi: 10.1016/j.jallcom.2019.152215.
[69] M. Sagawa, S. Fujimura, N. Togawa, H. Yamamoto, and Y. Matsuura, “New material for permanent magnets on a base of Nd and Fe (invited),” *J. Appl. Phys.*, vol. 55, no. 6, pp. 2083–2087, Mar. 1984, doi: 10.1063/1.333572.
[70] M. Okada, S. Sugimoto, C. Ishizaka, T. Tanaka, and M. Homma, “Didymium-Fe-B sintered permanent magnets,” *J. Appl. Phys.*, vol. 57, no. 8, pp. 4146–4148, Apr. 1985, doi: 10.1063/1.334647.
[71] W. Tang, S. Zhou, and R. Wang, “Preparation and microstructure of La-containing R-Fe-B permanent magnets,” *J. Appl. Phys.*, vol. 65, no. 8, pp. 3142–3145, 1989, doi: 10.1063/1.342711.
[72] C. Yan, S. Guo, R. Chen, D. Lee, and A. Yan, “Effect of Ce on the Magnetic Properties and Microstructure of Sintered Didymium-Fe-B Magnets,” *IEEE Trans. Magn.*, vol. 50, no. 10, pp. 1–5, Oct. 2014, doi: 10.1109/TMAG.2014.2322823.
[73] C. Yan *et al.*, “Enhanced Temperature Stability of Coercivity in Sintered Permanent Magnet by Substitution of Ce for Didymium,” *IEEE Trans. Magn.*, vol. 52, no. 5, pp. 1–4, May 2016, doi: 10.1109/TMAG.2015.2505244.
[74] J. Jin *et al.*, “Evolution of REFe2 (RE = rare earth) phase in Nd-Ce-Fe-B magnets and resultant Ce segregation,” *Scr. Mater.*, vol. 170, pp. 150–155, Sep. 2019, doi: 10.1016/j.scriptamat.2019.05.041.
[75] F. Chen *et al.*, “Investigation of the magnetic properties, microstructure and corrosion resistance of sintered Nd-Ce-Fe-B magnets with different Ce contents,” *J. Magn. Magn. Mater.*, vol. 557, p. 169477, Sep. 2022, doi: 10.1016/j.jmmm.2022.169477.
[76] Y. Enokido, A. Koda, Y. Umeda, D. Tanaka, and Y. Kitamoto, “Effect of grain-boundary phases in Y- and Ce-substituted R2Fe14B sintered magnets,” *J. Magn. Magn. Mater.*, vol. 517, p. 167406, Jan. 2021, doi: 10.1016/j.jmmm.2020.167406.
[77] X. Fan *et al.*, “Whole process metallurgical behavior of the high-abundance rare-earth elements LRE (La, Ce and Y) and the magnetic performance of Nd0.75LRE0.25-Fe-B sintered magnets,” *Acta Mater.*, vol. 154, pp. 343–354, Aug. 2018, doi: 10.1016/j.actamat.2018.05.046.
[78] X. Fan *et al.*, “A comparative study of NdY-Fe-B magnet and NdCe-Fe-B magnet,” *J. Rare Earths*, vol. 40, no. 9, pp. 1480–1487, Sep. 2022, doi: 10.1016/j.jre.2021.08.022.
[79] X. Fan *et al.*, “Core–shell Y-substituted Nd–Ce–Fe–B sintered magnets with enhanced coercivity and good thermal stability,” *Appl. Phys. Lett.*, vol. 110, no. 17, p. 172405, Apr. 2017, doi: 10.1063/1.4982679.

[80] W. Liu, Z. Zhang, M. Yue, Z. Li, D. Zhang, and H. Zhang, “Effects of La substitution on the crystal structure and magnetization of MM-Fe-B alloy (MM = La, Ce, Pr, Nd),” *J. Magn. Magn. Mater.*, vol. 464, pp. 61–64, Oct. 2018, doi: 10.1016/j.jmmm.2018.05.043.
[81] W. Gong and G. C. Hadjipanayis, “Misch-metal-iron based magnets,” *J. Appl. Phys.*, vol. 63, no. 8, pp. 3513–3515, 1988, doi: 10.1063/1.340726.
[82] E. Niu *et al.*, “Achievement of high coercivity in sintered R-Fe-B magnets based on misch-metal by dual alloy method,” *J. Appl. Phys.*, vol. 115, no. 11, p. 113912, Mar. 2014, doi: 10.1063/1.4869202.
[83] R. X. Shang *et al.*, “Structure and properties of sintered MM–Fe–B magnets,” *AIP Adv.*, vol. 7, no. 5, p. 056215, Jan. 2017, doi: 10.1063/1.4973603.
[84] Y. L. Liu *et al.*, “Intrinsic properties, phase constitution and microstructure of novel RE-Fe-B strip-casting alloys based on misch metal,” *J. Magn. Magn. Mater.*, vol. 513, p. 167162, Nov. 2020, doi: 10.1016/j.jmmm.2020.167162.
[85] X. Yu *et al.*, “Local profile dependence of coercivity in (MM0.3Nd0.7)-Fe-B sintered magnets,” *J. Magn. Magn. Mater.*, vol. 449, pp. 390–394, Mar. 2018, doi: 10.1016/j.jmmm.2017.10.048.
[86] W. Liu *et al.*, “MM-Fe-B based gap magnet with excellent energy density,” *Intermetallics*, vol. 115, p. 106626, Dec. 2019, doi: 10.1016/j.intermet.2019.106626.
[87] M. Zhu *et al.*, “Influence of Ce Content on the Rectangularity of Demagnetization Curves and Magnetic Properties of Re-Fe-B Magnets Sintered by Double Main Phase Alloy Method,” *IEEE Trans. Magn.*, vol. 50, no. 1, pp. 1–4, Jan. 2014, doi: 10.1109/TMAG.2013.2278018.
[88] S. X. Zhou, Y. G. Wang, and R. Ho/ier, “Investigations of magnetic properties and microstructure of 40Cedidymium–Fe–B based magnets,” *J. Appl. Phys.*, vol. 75, no. 10, pp. 6268–6270, May 1994, doi: 10.1063/1.355420.
[89] S. HUANG, H. FENG, M. ZHU, A. LI, Y. ZHANG, and W. LI, “Preparation of Sintered (Ce1−x Ndx)30FebalCu0.1B1 Magnets by Blending Powder Method,” *J. Iron Steel Res. Int.*, vol. 22, no. 7, pp. 598–601, Jul. 2015, doi: 10.1016/S1006-706X(15)30045-5.
[90] S. Huang, H. Feng, M. Zhu, A. Li, Y. Zhang, and W. Li, “Investigation of chemical composition and crystal structure in sintered Ce15Nd15FebalB1 magnet,” *AIP Adv.*, vol. 4, no. 10, p. 107127, Oct. 2014, doi: 10.1063/1.4898646.
[91] M. Zhu *et al.*, “An Enhanced Coercivity for (CeNdPr)–Fe–B Sintered Magnet Prepared by Structure Design,” *IEEE Trans. Magn.*, vol. 51, no. 11, pp. 1–4, Nov. 2015, doi: 10.1109/TMAG.2015.2451696.
[92] X. Fan *et al.*, “Tuning Ce distribution for high performanced Nd-Ce-Fe-B sintered magnets,” *J. Magn. Magn. Mater.*, vol. 419, pp. 394–399, Dec. 2016, doi: 10.1016/j.jmmm.2016.06.048.
[93] R. Han *et al.*, “Mechanism of the enhanced coercivity for the dual-main-phase Ce–Fe–B magnet,” *Sci. Rep.*, vol. 10, no. 1, p. 17975, Oct. 2020, doi: 10.1038/s41598-020-75082-w.
[94] Y. Zhang *et al.*, “Squareness factors of demagnetization curves for multi-main-phase Nd-Ce-Fe-B magnets with different Ce contents,” *J. Magn. Magn. Mater.*, vol. 487, p. 165355, Oct. 2019, doi: 10.1016/j.jmmm.2019.165355.
[95] H. Chen *et al.*, “Atomic scale insights into the segregation/partitioning behaviour in as-sintered multi-main-phase Nd-Ce-Fe-B permanent magnets,” *J. Alloys Compd.*, vol. 846, p. 156248, Dec. 2020, doi: 10.1016/j.jallcom.2020.156248.
[96] K. Zhu *et al.*, “Insight into the Property Enhancement Mechanism of Chemically Prepared Multi-Main-Phase (Nd,Ce)2Fe14B,” *ACS Appl. Mater. Interfaces*, vol. 12, no. 41, pp. 46549–46556, Oct. 2020, doi: 10.1021/acsami.0c13151.

[97] Y. Zhang *et al.*, "Post-sinter annealing influences on coercivity of multi-main-phase Nd-Ce-Fe-B magnets," *Acta Mater.*, vol. 146, pp. 97–105, Mar. 2018, doi: 10.1016/j.actamat.2017.12.027.
[98] J. Jin, M. Yan, Y. Liu, B. Peng, and G. Bai, "Attaining high magnetic performance in as-sintered multi-main-phase Nd-La-Ce-Fe-B magnets: Toward skipping the post-sinter annealing treatment," *Acta Mater.*, vol. 169, pp. 248–259, May 2019, doi: 10.1016/j.actamat.2019.03.005.
[99] W. Li, L. Zhao, and Z. Liu, "Micromagnetic simulation for the effects of core-shell distributions of RE on the magnetic properties of dual-main-phase Nd-Fe-B based magnets," *J. Magn. Magn. Mater.*, vol. 476, pp. 302–310, Apr. 2019, doi: 10.1016/j.jmmm.2018.12.107.
[100] J. Jin *et al.*, "Crucial role of the REFe2 intergranular phase on corrosion resistance of Nd-La-Ce-Fe-B sintered magnets," *J. Alloys Compd.*, vol. 735, pp. 2225–2235, Feb. 2018, doi: 10.1016/j.jallcom.2017.11.372.
[101] Q. Shi, Y. Liu, J. Li, W. Zhao, R. Wang, and X. Gao, "Significant improvement of the 2:14:1 phase formability and magnetic properties of multi-phases RE-Fe-B magnets with La substitution for Ce," *J. Magn. Magn. Mater.*, vol. 476, pp. 1–6, Apr. 2019, doi: 10.1016/j.jmmm.2018.12.043.
[102] J. Jin *et al.*, "Balancing the microstructure and chemical heterogeneity of multi-main-phase Nd-Ce-La-Fe-B sintered magnets by tailoring the liquid-phase-sintering," *Mater. Des.*, vol. 186, p. 108308, Jan. 2020, doi: 10.1016/j.matdes.2019.108308.
[103] Z. Wei, L. Ying, L. Jun, L. Lele, and G. Xi, "Role of lanthanum in microstructure evolution and enhanced magnetic properties of cerium-containing sintered magnets," *Mater. Werkst.*, vol. 51, no. 11, pp. 1561–1568, Nov. 2020, doi: 10.1002/mawe.202000021.
[104] H. Chen *et al.*, "Coercivity enhancement of Nd-La-Ce-Fe-B sintered magnets: Synergistic effects of grain boundary regulation and chemical heterogeneity," *Acta Mater.*, vol. 235, p. 118102, Aug. 2022, doi: 10.1016/j.actamat.2022.118102.
[105] H. Chen *et al.*, "Achievement of high performance in multi-main-phase (Pr,Nd,MM)-Fe-B sintered magnets by regulating microstructure," *Intermetallics*, vol. 124, p. 106870, Sep. 2020, doi: 10.1016/j.intermet.2020.106870.
[106] B. Peng, T. Ma, Y. Zhang, J. Jin, and M. Yan, "Improved thermal stability of Nd-Ce-Fe-B sintered magnets by Y substitution," *Scr. Mater.*, vol. 131, pp. 11–14, Apr. 2017, doi: 10.1016/j.scriptamat.2016.12.013.
[107] D. Liu *et al.*, "Exchange interaction and demagnetization process of high-abundance rare-earth magnets sintered using dual alloy method," *Sci. China Phys. Mech. Astron.*, vol. 65, no. 4, p. 247511, Feb. 2022, doi: 10.1007/s11433-021-1825-x.
[108] Z. Liu, J. He, and R. V. Ramanujan, "Significant progress of grain boundary diffusion process for cost-effective rare earth permanent magnets: A review," *Mater. Des.*, vol. 209, p. 110004, Nov. 2021, doi: 10.1016/j.matdes.2021.110004.
[109] K. Chen *et al.*, "Coercivity enhancement of (Nd,Ce)-Fe-B sintered magnets by doping Nd-Fe additives," *AIP Adv.*, vol. 7, no. 2, p. 025213, Feb. 2017, doi: 10.1063/1.4976722.
[110] F. Xia, Q. Sun, M. Zhu, Y. Wang, Y. Fang, and W. Li, "Novel design of self-compensated thermally stable Ce magnets without critical elements," *Mater. Des.*, vol. 216, p. 110590, Apr. 2022, doi: 10.1016/j.matdes.2022.110590.
[111] Y. J. Wong, H. W. Chang, Y. I. Lee, W. C. Chang, C. H. Chiu, and C. C. Mo, "Magnetic Properties of $Ce_{85}Al_{15}$ Doped NdFeB Sintered Magnet by Grain Boundary Diffusion of $Tb_{70}Cu_{30}$ Powders," *IEEE Trans. Magn.*, vol. 58, no. 8, pp. 1–5, Aug. 2022, doi: 10.1109/TMAG.2022.3144444.

[112] S. Fan *et al.*, “Grain boundary modification of multi-main-phase Nd0.7(La, Ce)0.3-Fe-B magnet towards 2 T coercivity,” *J. Alloys Compd.*, vol. 913, p. 165263, Aug. 2022, doi: 10.1016/j.jallcom.2022.165263.
[113] L. Zhang, Z. Li, Q. Ma, Y. Li, Q. Zhao, and X. Zhang, “Coercivity enhancement in (Ce,Nd)-Fe-B sintered magnets prepared by adding NdHx powders,” *J. Magn. Magn. Mater.*, vol. 435, pp. 96–99, Aug. 2017, doi: 10.1016/j.jmmm.2017.03.078.
[114] T. Ma *et al.*, “Enhanced coercivity of Nd-Ce-Fe-B sintered magnets by adding (Nd, Pr)-H powders,” *J. Alloys Compd.*, vol. 721, pp. 1–7, Oct. 2017, doi: 10.1016/j.jallcom.2017.05.257.
[115] J. Jin *et al.*, “Grain boundary engineering towards high-figure-of-merit Nd-Ce-Fe-B sintered magnets: Synergetic effects of (Nd, Pr)Hx and Cu co-dopants,” *Acta Mater.*, vol. 204, p. 116529, Feb. 2021, doi: 10.1016/j.actamat.2020.116529.
[116] T. Ma *et al.*, “Grain boundary restructuring of multi-main-phase Nd-Ce-Fe-B sintered magnets with Nd hydrides,” *Acta Mater.*, vol. 142, pp. 18–28, Jan. 2018, doi: 10.1016/j.actamat.2017.09.045.
[117] B. Peng, J. Jin, Y. Liu, Z. Zhang, and M. Yan, “Effects of (Nd, Pr)-Hx addition on the coercivity of Nd-Ce-Y-Fe-B sintered magnet,” *J. Alloys Compd.*, vol. 772, pp. 656–662, Jan. 2019, doi: 10.1016/j.jallcom.2018.09.084.
[118] Y. Liu, J. Jin, X. Wang, and M. Yan, “Comparison of (Pr, Nd)Hx grain boundary restructuring and diffusion on the magnetic properties of Nd–La–Ce–Fe–B sintered magnet,” *J. Alloys Compd.*, vol. 868, p. 159154, Jul. 2021, doi: 10.1016/j.jallcom.2021.159154.
[119] J. Jin *et al.*, “Concurrent improvements of corrosion resistance and coercivity in Nd-Ce-Fe-B sintered magnets through engineering the intergranular phase,” *J. Mater. Sci. Technol.*, vol. 110, pp. 239–245, May 2022, doi: 10.1016/j.jmst.2021.09.008.
[120] Y. Liu *et al.*, “A reliable route for relieving the constraints of multi-main-phase Nd–La–Ce–Fe–B sintered magnets at high La–Ce substitution: (Pr, Nd)Hx grain boundary diffusion,” *Scr. Mater.*, vol. 185, pp. 122–128, Aug. 2020, doi: 10.1016/j.scriptamat.2020.04.047.
[121] PARK K. T., “Effect of metal-coating and consecutive heat treatment on coercivity of thin Nd-Fe-B sintered magnets,” *Proc. 16th Int. Workshop Rare Earth Magn. Their Appl.*, vol. 257, 2000, [Online]. Available: https://cir.nii.ac.jp/crid/1573105974925324160
[122] K. Hirota, H. Nakamura, T. Minowa, and M. Honshima, “Coercivity Enhancement by the Grain Boundary Diffusion Process to Nd-Fe-B Sintered Magnets,” *IEEE Trans. Magn.*, vol. 42, no. 10, pp. 2909–2911, 2006, doi: 10.1109/TMAG.2006.879906.
[123] H. B. Feng, X. S. Chen, and A. H. Li, “Dual-shell core structure in grain boundary diffused high Ce content magnets with CeFe2 phase,” *J. Magn. Magn. Mater.*, vol. 522, p. 167493, Mar. 2021, doi: 10.1016/j.jmmm.2020.167493.
[124] M. Tang *et al.*, “Microstructure modification and coercivity enhancement of Nd-Ce-Fe-B sintered magnets by grain boundary diffusing Nd-Dy-Al alloy,” *J. Magn. Magn. Mater.*, vol. 442, pp. 338–342, Nov. 2017, doi: 10.1016/j.jmmm.2017.06.116.
[125] J. Wang, G. Wang, and D. Zeng, “Coercivity and corrosion resistance enhancement of multi-main-phase Nd-Ce-Fe-B sintered magnets by the grain boundary diffusion process using Pr81.5Ga19.5 and Pr81.5Ga14.5Cu5 alloys,” *J. Magn. Magn. Mater.*, vol. 503, p. 166639, Jun. 2020, doi: 10.1016/j.jmmm.2020.166639.
[126] M. Yan *et al.*, “Merits of Pr80Ga20 grain boundary diffusion process towards high coercivity–remanence synergy of Nd–La–Ce–Fe–B sintered magnet,” *Acta Mater.*, vol. 231, p. 117873, Jun. 2022, doi: 10.1016/j.actamat.2022.117873.

[127] R. Du *et al.*, “Coercivity enhancement of the sintered Nd-Ce-Fe-B magnet via grain boundary diffusion with Tb70Fe30 alloy,” *J. Magn. Magn. Mater.*, vol. 551, p. 169034, Jun. 2022, doi: 10.1016/j.jmmm.2022.169034.
[128] F. Chen *et al.*, “Coercivity enhancement of a Ce-based permanent magnet by grain boundary diffusion with Re70Cu30 (Re: Nd/Dy) eutectic alloys,” *J. Alloys Compd.*, vol. 819, p. 152965, Apr. 2020, doi: 10.1016/j.jallcom.2019.152965.
[129] J. Jin, W. Chen, M. Li, X. Liu, and M. Yan, “PrAl and PrDyAl diffusion into Nd-La-Ce-Fe-B sintered magnets: Critical role of surface microstructure in the magnetic performance,” *Appl. Surf. Sci.*, vol. 529, p. 147028, Nov. 2020, doi: 10.1016/j.apsusc.2020.147028.
[130] Y. Liu, J. He, H. Yu, Z. Liu, and G. Zhang, “Restoring and enhancing the coercivity of waste sintered (Nd,Ce,Gd)FeB magnets by direct Pr–Tb–Cu grain boundary diffusion,” *Appl. Phys. A*, vol. 126, no. 8, p. 657, Aug. 2020, doi: 10.1007/s00339-020-03857-z.
[131] Z. Li *et al.*, “Effect of inhibiting CeFe2 on grain boundary diffusion of Ce/La-Ce containing Nd-Fe-B magnets,” *Mater. Lett.*, vol. 261, p. 127017, Feb. 2020, doi: 10.1016/j.matlet.2019.127017.
[132] Q. Zhu *et al.*, “Coercivity enhancement of sintered Ce-substituted Nd-Fe-B magnets by grain boundary diffusion process of Tb,” *J. Magn. Magn. Mater.*, vol. 515, p. 167274, Dec. 2020, doi: 10.1016/j.jmmm.2020.167274.
[133] L. Zhang *et al.*, “The technology and mechanism of coercivity promotion of Ce-rich dual-main-phase sintered magnets,” *J. Magn. Magn. Mater.*, vol. 490, p. 165414, Nov. 2019, doi: 10.1016/j.jmmm.2019.165414.
[134] T. Saito, T. Takeuchi, and H. Kageyama, “Structures and magnetic properties of Nd-Fe-B bulk nanocomposite magnets produced by the spark plasma sintering method,” *J. Mater. Res.*, vol. 19, no. 9, pp. 2730–2737, 2004, doi: 10.1557/JMR.2004.0358.
[135] X. G. Cui *et al.*, “Magnetic properties, thermal stability, and microstructure of spark plasma sintered multi-main-phase Nd-Ce-Fe-B magnet with PrCu addition,” *J. Alloys Compd.*, vol. 822, p. 153612, May 2020, doi: 10.1016/j.jallcom.2019.153612.
[136] L. He *et al.*, “Hybrid Effect of Exchange Coupling in Ce–Pr–Nd–Fe–B SPSed Magnets by Adding Pr–Fe–B Alloys,” *IEEE Trans. Magn.*, vol. 57, no. 3, pp. 1–7, Mar. 2021, doi: 10.1109/TMAG.2020.3037844.
[137] X. G. Cui *et al.*, “Enhanced magnetic properties and thermal stability of spark plasma sintered multi-main-phase Nd-Ce-Fe-B magnet via co-adding DyF3 and Cu,” *J. Alloys Compd.*, vol. 902, p. 163786, May 2022, doi: 10.1016/j.jallcom.2022.163786.
[138] Q. Jiang *et al.*, “Special microstructure evolution and enhanced magnetic properties of Ce-Fe-B-based spark plasma sintered magnets with core-shell structure by NdCu addition,” *J. Alloys Compd.*, vol. 775, pp. 449–456, Feb. 2019, doi: 10.1016/j.jallcom.2018.10.114.
[139] S. Pandian, V. Chandrasekaran, G. Markandeyulu, K. J. L. Iyer, and K. V. S. Rama Rao, “Effect of Al, Cu, Ga, Nb additions on the magnetic properties and microstructural features of sintered NdFeB,” *J. Appl. Phys.*, vol. 92, no. 10, pp. 6082–6086, 2002, doi: 10.1063/1.1513879.
[140] E. J. Skoug, M. S. Meyer, F. E. Pinkerton, M. M. Tessema, D. Haddad, and J. F. Herbst, “Crystal structure and magnetic properties of Ce2Fe14−xCoxB alloys,” *J. Alloys Compd.*, vol. 574, pp. 552–555, Oct. 2013, doi: 10.1016/j.jallcom.2013.05.101.
[141] M. Jurczyk and W. E. Wallace, “Magnetic behavior of R1.9Zr0.1Fe14B and R1.9Zr0.1Fe12Co2B compounds,” *J. Magn. Magn. Mater.*, vol. 59, no. 3, pp. L182–L184, Jun. 1986, doi: 10.1016/0304-8853(86)90409-9.

[142] M. Jurczyk, “Nd1.9M0.1Fe12Co2B, M = Ti or Hf as a material for permanent magnets,” *J. Magn. Magn. Mater.*, vol. 67, no. 2, pp. 187–189, Jun. 1987, doi: 10.1016/0304-8853(87)90228-9.
[143] B. J. Ni, H. Xu, X. H. Tan, and X. L. Hou, “Study on magnetic properties of Ce17Fe78−xZrxB6 (x=0–2.0) alloys,” *J. Magn. Magn. Mater.*, vol. 401, pp. 784–787, Mar. 2016, doi: 10.1016/j.jmmm.2015.10.110.
[144] Q. Jiang *et al.*, “Magnetic properties and microstructure of melt-spun Ce17Fe78−xB6Hfx (x=0–1.0) alloys,” *J. Magn. Magn. Mater.*, vol. 444, pp. 344–348, Dec. 2017, doi: 10.1016/j.jmmm.2017.08.068.
[145] L. Yin, J. Yan, B. C. Sales, and D. S. Parker, “Critical-Element-Free Permanent-Magnet Materials Based on ${\mathrm{Ce}}_{2}{\mathrm{Fe}}_{14}\mathrm{B}$,” *Phys. Rev. Appl.*, vol. 17, no. 6, p. 064020, Jun. 2022, doi: 10.1103/PhysRevApplied.17.064020.
[146] P. de Rango, F. N. Genin, D. Fruchart, A. Traverse, S. Rivoirard, and I. Popa, “Localisation of Zr in Nd–Fe–B alloys,” *Proc. Int. Conf. Magn. ICM 2000*, vol. 226–230, pp. 1377–1378, May 2001, doi: 10.1016/S0304-8853(00)00914-8.
[147] L. Q. Yu, X. L. Zhong, Y. P. Zhang, Y. G. Yan, Y. H. Zhen, and M. Zakotnik, “Production and corrosion resistance of NdFeBZr magnets with an improved response to thermal variations during sintering,” *J. Magn. Magn. Mater.*, vol. 323, no. 9, pp. 1152–1155, May 2011, doi: 10.1016/j.jmmm.2010.12.029.
[148] M. Itakura *et al.*, “Suppression mechanism of abnormal grain growth by Zr addition in pressless processed Nd-Fe-B sintered magnets,” *J. Alloys Compd.*, vol. 887, p. 161244, Dec. 2021, doi: 10.1016/j.jallcom.2021.161244.
[149] J. S. Zhang *et al.*, “Improving the hard magnetic properties by intragrain pinning for Ta doped nanocrystalline Ce-Fe-B alloys,” *J. Mater. Sci. Technol.*, vol. 35, no. 9, pp. 1877–1885, Sep. 2019, doi: 10.1016/j.jmst.2019.05.007.
[150] L.-L. Zhang *et al.*, “Uneven Evolution of Microstructure, Magnetic Properties and Coercivity Mechanism of Mo-Substituted Nd–Ce–Fe–B Alloys,” *Acta Metall. Sin. Engl. Lett.*, vol. 34, no. 4, pp. 590–596, Apr. 2021, doi: 10.1007/s40195-020-01079-z.
[151] K. Orimoloye, D. H. Ryan, F. E. Pinkerton, and M. Medraj, “Intrinsic Magnetic Properties of Ce2Fe14B Modified by Al, Ni, or Si,” *Appl. Sci.*, vol. 8, no. 2, 2018, doi: 10.3390/app8020205.
[152] D. Li and Y. Bogatin, “Effect of composition on the magnetic properties of (Ce1−xNdx)13.5 (Fe1−y−zCoySiz)80B6.5 sintered magnets,” *J. Appl. Phys.*, vol. 69, no. 8, pp. 5515–5517, Apr. 1991, doi: 10.1063/1.347985.
[153] J. S. Zhang *et al.*, “Suppressing the CeFe2 phase formation and improving the coercivity and thermal stability of Ce-Fe-B alloys by Si substitution,” *Intermetallics*, vol. 107, pp. 75–80, Apr. 2019, doi: 10.1016/j.intermet.2019.01.013.
[154] M. Jurczyk, “Effect of substitution of Al and Mo on the magnetic properties of R2Fe12−xTxCo2B (R=synthetic mischmetal, didymium and neodymium),” *J. Magn. Magn. Mater.*, vol. 73, no. 2, pp. 199–204, Jun. 1988, doi: 10.1016/0304-8853(88)90293-4.
[155] J. Zhang *et al.*, “Enhanced hard-magnetic properties and thermal stability of nanocrystalline Ce-rich Ce-Fe-B alloys by combining La substitution and Si addition,” *J. Magn. Magn. Mater.*, vol. 552, p. 169217, Jun. 2022, doi: 10.1016/j.jmmm.2022.169217.
[156] C. Zhou, M. Pan, Q. Wu, and H. Yang, “Improvement of magnetic properties for Ti doped Ce-Fe-B alloys: Effectively inhibiting CeFe2 phase formation,” *J. Magn. Magn. Mater.*, vol. 502, p. 166564, May 2020, doi: 10.1016/j.jmmm.2020.166564.

[157] S. U. Rehman *et al.*, “Phase constituents, magnetic properties, intergranular exchange interactions and transition temperatures of Ge-doped CeFeB alloys,” *J. Phys. Chem. Solids*, vol. 132, pp. 182–186, Sep. 2019, doi: 10.1016/j.jpcs.2019.04.033.
[158] Q. Jiang *et al.*, “Effect of Ga addition on the valence state of Ce and magnetic properties of melt-spun Ce17Fe78-xB6Gax (x = 0-1.0) ribbons,” *AIP Adv.*, vol. 7, no. 8, p. 085013, Aug. 2017, doi: 10.1063/1.5000703.
[159] L. Xi *et al.*, “Dependence of magnetic properties on microstructure and composition of Ce-Fe-B sintered magnets,” *J. Rare Earths*, vol. 37, no. 8, pp. 865–870, Aug. 2019, doi: 10.1016/j.jre.2018.11.013.
[160] Y. M. Tao *et al.*, “Cu-mediated grain boundary engineering in Nd–Ce–Fe–B nanostructured permanent magnets,” *Mater. Today Nano*, vol. 19, p. 100230, Aug. 2022, doi: 10.1016/j.mtnano.2022.100230.
[161] Z. Y. Zhang, L. Z. Zhao, X. C. Zhong, D. L. Jiao, and Z. W. Liu, “Phase precipitation behavior of melt-spun ternary Ce2Fe14B alloy during rapid quenching and heat treatment,” *J. Magn. Magn. Mater.*, vol. 441, pp. 429–435, Nov. 2017, doi: 10.1016/j.jmmm.2017.06.028.
[162] J. S. Zhang *et al.*, “Enhancement in hard magnetic properties of nanocrystalline (Ce,Y)–Fe–Si–B alloys due to microstructure evolution caused by chemical heterogeneity,” *J. Mater. Chem. C*, vol. 8, no. 42, pp. 14855–14863, 2020, doi: 10.1039/D0TC03011B.